Submitted to Studies of High Temperature Superconductors, NOVA Science NY,
June 2001, A.V.Narlikar and F.M.Araùjo-Moreira ed.s
preprint at: http://ing.univaq.it/energeti/Research/Fisica/supgru.htm

THE JOSEPHSON JUNCTION ARRAYS AS MODEL FOR GRANULAR HTC SUPERCONDUCTORS

Cinzia De Leo and Giacomo Rotoli^
Dipartimento di Energetica and ^INFM, Università di L'Aquila
Località Monteluco, I67040 Roio Poggio, L'Aquila, ITALY.

1.INTRODUCTION.

It was very soon after the discovery of HTC superconductivity than their unusual properties were described in term of Josephson junction arrays (JJA). First analyses indicate the presence of a complex structure which manifests in the form of glass state, irreversible behavior, and material inhomogeneity as granularity [1]. Historically the presence of "strong" and "weak" Josephson coupling between Grain Boundary (GB) was introduced by Chaudari et al. [2]. On the other hand JJA was just studied as they stand or like model of some granular (LTC) film. Seminal work of Lobb, Abraham and Tinkham [3] and the first self-consistent model equations derived by Nakajima and Sawada [4] was among the most important investigations in the first eighties. Along nineties until recently LTC JJA was thought essentially as prototype for new most efficient and powerful oscillators with frequencies above 100 GHz. Most of the recent JJA device physics was developed in this perspective [5].

The behavior of JJAs is intriguing also in view of their analogy with II type superconductors. In fact is well-known that Josephson junctions carry vortex states over a length which depends on their critical current the so-called Josephson penetration length λ_J. In continuos structures as Long Josephson junctions (LJJ) this length is the typical distance over which Josephson vortices extends in the system. So a (long) Josephson junction can shown phenomena like Meissner effect, vortex excitations and pinning, until the set up of a critical state [6]. These phenomena happens at a scale which is different of some order of magnitudes by that of II type superconductor in which is the behavior of the Abrikosov vortex excitations that influence the critical phenomena. This justify the name "weak" superconductivity somewhat associated with Josephson junctions. So in the study of physics of HTC materials very often both descriptions based on JJA and Ginzburg-Landau equations (GL) have been used and compared. In discrete structures, as most build

and analyzed JJA, is the ratio between the structure (mean) lattice space and the (mean) Josephson length l_J, i.e., the mean vortex dimension, that is of fundamental importance for their static and dynamical properties. The square of this ratio is called b_L and its inverse is the analogous of Josephson penetration length for discrete structures. The phenomena reported above, as pinning and critical state, continue to exist also for strongly discrete systems. The most impressive signature is the presence of Bean [7] or Bean-like penetration of the magnetic field in JJA for strongly discrete arrays.

First simplest models treat one-dimensional arrays in which loops with no more than two Josephson junctions are separated by holes representing the intergrain space (cf. Fig.1a). Statics and dynamics of such systems can be well represented by so-called Discrete Sine-Gordon equation (DSG) as is shown in Vaccarone and Parodi [8] or by its well-known continuos limit the Sine-Gordon (SG) equation extensively treated with regards to pinning properties by Fehrenbecher, Geshkenbein and Blatter [9]. However soon one-dimensional models were left for more complexes arrays the so-called two-dimensional arrays in which three or four Josephson junctions form the basic building block around the hole (cf. Fig.1b). The behavior of a 2D matrix of superconducting grains can be approximated by a two-dimensional regular array of Josephson junctions. Most studies have been dedicated to this model among this we remember Majhofer, Wolf and Dieterich [10], Petraglia, Filatrella and Rotoli [11] based on the same simple approach of next-neighbor meshes used in Nakajima and Sawada [4]. Most sophisticated and complete model that include the full mutual inductance matrix have been developed by Dominguez and José [12], Phillips et al. [13], and Reinel et al. [14], though numerically heavy this last model is the only correct description for the current flowing into the arrays in particular when the system is strongly discrete. Extension to 3D models have been also described both in term of simplified approaches, e.g. see Auletta, De Luca, Pace and Raiconi [15], and in the simplest full 3D configurations, e.g. see De Luca, Pace, Auletta and Raiconi [16] and again more recently De Luca et al. [17]. These last approaches regard mainly the magnetization properties of such JJA, but are not lacking also studies in dynamics [18].

An important branch of studies was dedicated to investigate the presence of so-called Berezinskii-Kosterlitz-Thouless (BKT) transition, i.e., the unbinding of vortex-antivortex pairs. JJA was known as one of most approachable models in which BKT transition can be found [19]. Recent studies, e.g., see Herbert et al. [20], have shown how finite size effect and the presence of free vortex in JJA influences the vortex unbinding mechanism. This is of great interest because a BKT transition would be occur in HTC materials, as was shown at the end of eighties, e.g. see Martin et al. [21] for BSSCO, Yeh and Tsuei, Ying and Kwok [22] for YBCO. So this can be the field for a fruitful quantitative comparison between HTC and LTC physics. Other numerical experiments on vortex phase transition was performed on 3D JJA have been made by Chen and Teitel which have treated the vortex lattice melting transition [23] and by Bokil and Young which study the vortex-glass transition [24].

On the other hand it is worth to note that from a theoretical point of view 2D system of superconducting grain connected by Josephson junctions, i.e., the prototype 2D array, is a very attractive system for test the physics of so-called Hubbard-Bose systems (HB) (cf. the works of M.Fisher and Grinstein, and, M.Fisher, Grinstein, Weichman and D.Fisher [25]). So many studies have been made to demonstrate the existence of phase-transitions connected with the HB model [26]. Such investigations have been proved to be of great interest for LTC arrays. For example one of the most relevant was the experimental

evidence of a Mott transition in 2D arrays obtained by van Oudenaarden and Mooji [27]. For true HTC systems the importance of HB model is hard to decide when the theoretical models, e.g. the XY model [28] often invoked for 2D arrays, are usually different from real model of HTC. These show higher self–induced fields or strong positional disorder that tend to hinder the subtler phase transition effects (cf. ref. [25] for the effect of disorder on the Mott transition). Anyway, as we cite below, the progress toward so-called "engineered" HTC materials can constitute a significant breakthrough in this field also in view of the study of quantum and/or statistical properties of such systems.

Disordered JJA was studied very early also in relation to HTC superconductors in the continuos case in the above-mentioned ref.[9] in 1D case and by Leath and Xia [29] in 2D case. In ref.[9] the basic model is the inhomogeneous LJJ, i.e., the limit for small loop inductance of 1D JJA which implies that system is described by a disordered SG equation. In particular the LJJ is described by a position dependent Josephson current giving arise to pinning of fluxons and to a critical current density. In ref.[29] zero temperature overdamped disordered arrays was studied using a model which basically reproduce the XY model without self-induced flux. There were many recent studies on disorder in the XY model: diluted XY model with percolation was studied by Granato and Dominguez [30]. Another XY based study was performed by Mombelli and Beck [31] that evaluated the complex impedance of a disordered array.

Anyway disorder was not the whole story of HTC materials. For perhaps surprising reasons the recent and most promising applications all came from the discovery that at very low scale, typically submicron scales, HTC are possibly not disordered materials due to their strongly anisotropy in the crystalline structure. In such sense the first breakthrough was made with the discovery of so-called intrinsic Josephson effect in BSSCO by Kleiner, Steinmeyer, Kunkel and Müller [32] and successively found also in other HTC materials (see Kleiner and Müller [33]). Intrinsic junctions are very promising for the developing of new submicron HTC devices. It is worth to note that intrinsic junctions in BSSCO layers can be described as stacked junction arrays, these are nothing but a stack of 1D arrays [34]. Today "engineered" structures and/or "intrinsic" clean structures are probably the most important current of studies in device oriented HTC materials. Often "intrinsic" Josephson junctions are accessed by sophisticated fabrication technology [35]. So also the distinction between "engineered" and "intrinsic" structures tends to be loose, especially when submicron structures have to be accessed and used as superconducting electronic devices. On the other hand also the penetration of the magnetic field and the pinning is subject to "engineering". Regular arrays of pinning centers can be introduced directly in HTC materials or in some LTC model material as magnetic dots or defects [36]. The interest in these structures is that they can produce strong pinning so giving higher critical currents. Both experiments, e.g., see Gray, Field and Miller [37] and theoretical investigations, e.g. Nori et al. [38], argue that periodic or more generally weak disorder plus periodicity, can enhance strongly the pinning.

In this work we show two cases in which JJA model of HTC superconductors can give new useful insights in the physics of these materials. Both problems are closely linked to the nature of Josephson coupling along the GBs. Is the coupling "strong" or "weak", and, there is some other aspect which characterize its properties, as so-called π-junctions?

Firstly we treat 1D arrays at light of recent analysis on the flux penetration along percolation paths in YBCO films and bulks. In recent years most literature was dedicated to the question of magnetic properties of YBCO and especially the way in which magnetic

flux penetrate in it. Most studies concentrate on the analysis of Grain Boundary (GB) surface between YBCO crystals as the place where the flux penetration occurs (e.g., see the very impressive magneto-optical images reported in Feldmann et al. [39] for YBCO films). This was the last achievement of a long series of analysis regarding the effect of so-called misorientation angle started just after the discovery of HTC materials [40]. Characterization of magnetic properties of YBCO bicrystals was given by many authors among this Gurevich and Cooley for bulk YBCO [41], which explicitly talk of preferential flux quanta motion along percolative path with pinning centers, and the University of Wisconsin group [42] which analyze the properties of intergrain currents for different misorientation angles in YBCO bicrystal films showing how Josephson weak link properties sets on for angles larger than about 7 degrees. Mechanisms at the intergrain boundary were analyzed also by Evetts et al. [43], Maggio-Aprile et al. [44] and Cai et al. [45]. Recently Gray [37] have explained the higher critical currents found in the films with an "intrinsic" local order due to meandering of GB at submicron scale (about 200-800 nm), meanders will act just like a naturally engineered pinning center array to enhance the critical current. This idea is not new because the pinning properties of regular arrays of defects are well-known (see for example ref.s [9]-[38]). An analysis of YBCO films in terms of Josephson junctions with random length distribution was made by G.Ghigo et al. [46], but they analyze uncorrelated independent junctions. Further analysis show that these junctions develop on very small-scale [47] thus implying the observed high critical fields. An attempt to a description in term of strongly discrete 1D JJA, i.e., formed by almost uncoupled point-like junctions, somewhat analogue to first model of Vaccarone and Parodi [8], was recently made by G.Rotoli et al. [48] where we observe the critical current "plateau"-like dependence on the magnetic field. Below in sect.3 we will try to improve it introducing inhomogeneity and weak disorder and discussing its pinning properties.

As second case we treat the so-called Paramagnetic Meissner Effect (PME) in two-dimensional JJA. PME, somewhat called also Wohllenben Effect, was found in field cooled HTC samples by Braunisch et al. [49]. Very soon Sigrist and Rice [50] justify the effect invoking the d-wave symmetry of HTC materials, i.e., PME would be a signature for d-wave superconductivity. This will reflects in the presence of so-called π-junctions for some of the GBs in the array meshes. Early numerical simulations made by Dominguez, Jagla and Balseiro [51] in two-dimensional arrays seems give a qualitative confirmation the role of π-junctions in producing PME states. Anyway soon the effect was discovered also in traditional Nb LTC superconductors by Thompson et al. [52] questioning the link with d-wave symmetry. Other observation in LTC superconductors was made also by Kostic et al. and Geim et al. [53] thus confirming the existence of the effect. First explanation of PME in LTC superconductors involve non-equilibrium flux configurations as flux-compression or giant vortex states (cf. Koshelev and Larkin, Moschalkov et al., and Deo et al. [54]) or surface barrier states (cf. Deo et al. [55]). Reentrant AC susceptibility was observed in 2D JJA by P.Barbara et al., and by Araùjo-Moreira et al. [56]. These were the first indications of the paramagnetic behavior of 2D JJA. PME effect was systematically observed studying the AC susceptivity by W.A.C.Passos et al. in 3D disordered arrays fabricated using powders of both HTC and LTC superconductors [57]. Very recently (DC) PME was observed in LTC 2D arrays by A.P.Nielsen et al. [58] using a Scanning Squid Microscope (SSM). In this work also a new explanation for PME was attempted: multiply connected superconductors generate paramagnetism because circulation of the currents at boundaries

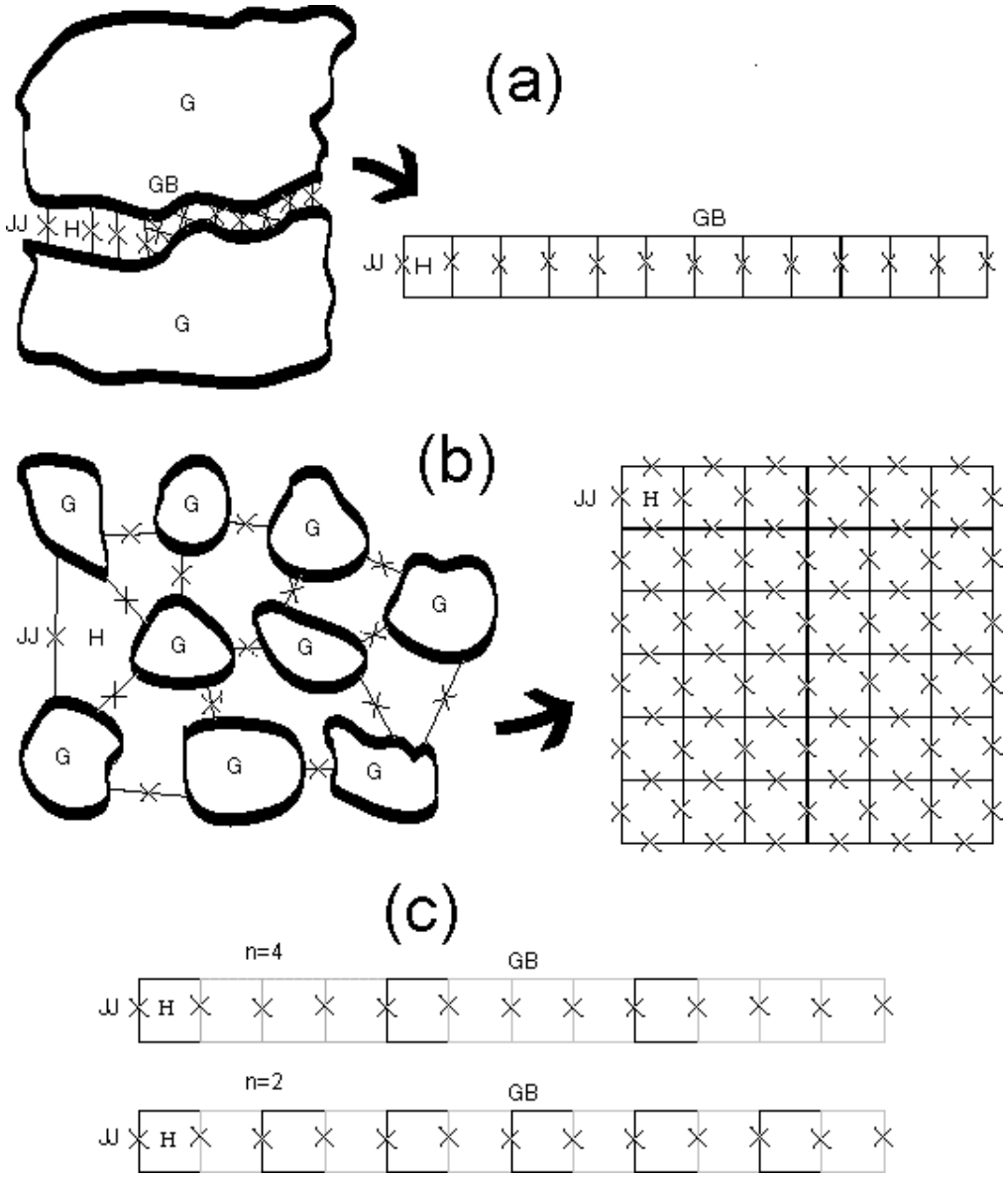

Fig.1 Typical JJAs model based on granular material structure: (a) 1D JJA modeling the GB between two (relatively) large superconducting island (G), the holes (H) separate the Josephson channels (junctions, JJ); (b) 2D JJA modeling a strongly discrete material made of many superconducting island (G), holes (H) are surrounded by a junctions (JJ) loop; (c) 1D array with periodical variation of parameter b_L the case n=2 and n=4 are shown.

after field cooling favor the presence of paramagnetic loops in the interior of the sample. This theory was confirmed by numerical simulations of the full inductance matrix model of 2D arrays by De Leo et al. [59]. Here we will review the arguments giving some new results from simulation of square 20x20 arrays, discussing the analytical relation with 1-mesh case and briefly treating the dependence of PME states on the screening properties of

the array. We will consider PME in sect.4; next section will be dedicated to derive a JJA general self-consistent model.

2. MODEL

JJA are described as discrete structures in which N Josephson junctions around a loop form an elementary building block. In Fig.1 a general granular object is analyzed in term of this model. The (closed) sets of superconducting path separating two homogeneous regions in the material represent the so-called superconducting islands or grain (G). Tunneling of Cooper pairs between grains indicate that supercurrents are present and so Josephson channels. We do not make hypothesis on the nature of junctions, simply assume that they can be modeled by usual Josephson equations. The JJA models treated here is circuital, i.e., the variation of the order parameter in the granular superconductor formed by the islands is concentrated along the GB regions so permitting the description in terms of properties of the circuit formed by superconducting path along the GB which carry inductances, and the local properties of the intergranular coupling itself such as local Josephson supercurrent, plus capacitance and dissipation, if, as usual the junctions are analyzed in term of the simple so-called RSJ model. As is shown in Fig.1a a percolative path, i.e. a GB, separating two large islands (G) can be mapped over 1D arrays, where "holes" (H) simply represents regions of poor and/or absent tunneling between adjacent islands and "junctions" (JJ), marked by a cross, represents regions where the supercurrents can flow. With a higher granularity the model take the most common form of a 2D array as is shown in Fig.1b where holes are the intergranular voids in the superconductors. So by 2D (regular) array we mean a Josephson coupling in both x and y directions whereas in 1D arrays the Josephson coupling is just in one spatial direction. This classification scheme follows that of Barahona et al. [60]. 3D models can be defined in similar way. It is obvious just from here that it is a matter of scale which models, 1D, 2D or 3D, is the most suitable for a given problem: fine description of percolative path between single GBs can be more conveniently described as 1D arrays, whereas the coarse-grain behavior of a large amount of islands is well described by 2D models. Often this means that in such "discrete" 2D models, though one would in principle describe each island with a GL type equation for its order parameter, it can be assumed that island order parameter have a single value for the whole island. This is usual in the case of XY model where the phase of the order parameter is the island "spin" [28]. On the other hand models where screening currents, generated by local inductances, occur permit a local variation of the order parameter phases along the boundary of the array islands. The most simplest model in these respects is the continuous 1D model, i.e., the LJJ, where screening effects remain finite because the mesh dimension goes to zero together with the mesh flux, leading to the well-known SG model.

The general deduction of the equations describing the above-described JJA is performed via the following steps. Phillips et al. [13], Dominguez and José [12], Lucheroni [61] and Petraglia, Filatrella and Rotoli [62] give examples of general deduction for 2D JJA model with slight differences. 1D JJA is generally deduced as a different model though the basics ingredients to deduce their equations are essentially the same. However it is worth to note that 1D and 2D models can differs greatly also in their static properties (e.g. see Grimaldi et al. [63]). We note that in the array terminology there are many different terms that substantially indicate the same thing: mesh, loop, plaquette, cell and hole all indicate the closed superconducting paths interrupted by two or more junction that form the array. In

the following we use the term mesh in the formal deduction of equations, and loop whenever the term is more appropriate for physical insight.
If the junctions are present in any branch of the array then the branch number represents the number of degree of freedom of the system. In general a rectangular N_cxN_r square-mesh JJA have a number of $2N_cN_r+N_r+N_c$ branches. For a triangular array made of triangular-mesh with N rows the number is 3N(N+1)/2. Here we deduce the equations for square-mesh arrays because is the model mostly studied in literature, but procedure is in principle valid for any type of arrays so results valid for square-mesh is also valid in arbitrary geometry for array meshes. We limit to give some hint for the particular cases of triangular and 1D arrays. In order to deduce the equations describing the arrays we must remember that for each of the N_cxN_r loops we can write the fluxoid quantization in the following form:

$$\sum_{loop} j_k = 2p\, n_k - \frac{2p}{\Phi_0} f_{tot,k} \tag{1}$$

where j_k are the (oriented) phases of the Josephson junctions along the kth loop; n_k an integer quantum number; $f_{tot,k}$ the flux threading in the loop and Φ_0 the flux quantum. In general $f_{tot,k}$ is given by the sum of $f_{ext,k}$, i.e. the external flux in the loop, plus the possible flux noise terms $f_{noise,k}$, and finally plus the flux $f_{induced,k}$ which is the flux generated by JJA itself. Separating these terms and rewriting the Eq.(1) in vector form:

$$-\mathbf{M}\vec{j} = 2p\,\vec{n} - 2p\,\vec{f}_{ext} - 2p\,\vec{f}_{noise} - \frac{2p}{\Phi_0}\vec{f}_{induced} \tag{2}$$

where **M** is the matrix performing the oriented sum of the phases in each loop (the reason of minus sign in front of **M** will be clear below); f_{ext} and f_{noise} are the so-called frustrations defined as f/Φ_0, here separated in the external flux and the external flux noise. The vector signs substitute the index k for all quantities. We note that rank(**M**)=N_cxN_r. Another set of equations is derived by current conservation at any of its (N_c+1)x(N_r+1)-1 independent nodes. In vector form this reads:

$$\mathbf{R}\mathbf{I}_b = \mathbf{I}_f \tag{3}$$

where **R** is the matrix with rank(**R**)=(N_c+1)x(N_r+1)-1 giving the current conservation rules at each node and $\mathbf{I}_b$ is the vector of the branch currents. The vector $\mathbf{I}_f$ represents an external bias current. We note that the sum of the matrix ranks, i.e., the number of independent equations written in Eq.(2) and Eq.(3), is (N_c+1)x(N_r+1)-1+N_cxN_r=2N_cxN_r+N_r+N_c is just equal to the number of degree of freedom of the system. This means that in order to find the phases of all the junctions the sets of Eq.s (2) and (3) are all we need. We note that the same two equations are valid for triangular arrays if in Eq.(2) the sum over phases spans over three rather than four junctions and Eq.(3) gives the current conservation at the nodes for such arrays (so matrixes **M** and **R** are different). Moreover the same equations can be used for 1D arrays if the current conservation is imposed to the top row of nodes, so that 1D arrays have N=N_c+1 branches containing a Josephson junctions, and in Eq.(2) the sum

spans only over the two junctions present in the mesh (here is just sufficient to known the equations for the branch containing Josephson junctions). Anyway in order to solve the system formed by Eq.s (2) and (3) we need to know how the JJA responds to the magnetic external flux appearing in Eq.(2), i.e., how the term ϕ_{induced} is linked to the currents. If no flux is generated by the array Eq.(2) is a constraint that permits to reduce the degree of freedom to the system. This is a very special case and from a circuital point of view means that no inductance is present in any loops or more properly the inductance are negligible. Will be shown below by means of a simple transformation of variables that this special case maps exactly over the XY model. In the general case the array always generate some flux this is due to the circulation of some screening currents in the arrays when the array is magnetized. This flux is referred often as Self-Induced Magnetic Field (SIMF) [12] or simply the self-field effect [13]. On general ground the flux induced in a given loop depends on the currents in all others branches via an expression of the form:

$$\vec{f}_{induced} = L_{mean}\mathbf{L}\mathbf{I}_b \tag{4}$$

where **L** is the (normalized) branch-loop mutual inductance matrix of the array. Here L_{mean} represents the mean self-inductance of the array loops which here acts as normalizing factor for matrix **L**. Depending on the number of terms we want keep in **L** we talk of next-neighbors models when we retain only few near-diagonal terms due to the adjacent meshes or full mutual inductance model when we retain all the terms, i.e., any loop of the array is coupled via mutual inductances to all other loops. The basic model, which retains only the self-inductance, i.e., matrix **L** will be proportional to **M**, will be called self-inductance model. The decision on which model is more appropriate depends on the intensity of the screening as we shown below, but it is worth to say that in presence of strongly disordered arrays the screening can be high in some regions of the array and low in other. Anyway we can safely say that surely the screening is higher in 2D arrays than in 1D because of large number of loops contributing to the flux in 2D case. Moreover 1D arrays, as explained above, are the most suitable to describe fine details thus giving a smaller geometrical self-inductance and so a lower screening. To combine Eq.s (2), (3) and (4) in a single set of equations, we need to decide how to define the so-called screening (or mesh) currents. This is somewhat arbitrary because exist different sets of possible screening current, due to the fact that they are only $N_c x N_r$, anyway this choice is irrelevant because after substitutions are made screening currents disappears from equations. Typical choice for four junctions loops in 2D JJA, in absence of bias currents, is for example:

$$I_b^k = d_h\left(I_s^{i,j} - I_s^{i,j-1}\right) + d_v\left(I_s^{i-1,j} - I_s^{i,j}\right) \tag{5}$$

where d_h or d_v are Kronecker operators equal respectively to one (zero) if the branch is horizontal (vertical) and viceversa; I_s represents the screenings currents in the meshes adjacent to the k-th branch here indexed with row-column superscripts. On the other hand for two junction meshes in 1D JJA the most obvious choice is the following:

$$I_b^k = I_s^{i,j} - I_s^{i,j-1} \tag{6}$$

where the screening currents I_s are circulating in the two meshes adjacent to the k-th branch. These choices are ways to satisfy the homogeneous part of Eq.(3) automatically, i.e., the (Nc+1)x(Nr+1)-1 node equations are compatible with Eq.(5) or (6) at each node. However in general a solution of Eq.(3) is given by the sum of a solution of homogeneous equation, i.e., $\mathbf{RI}_b=\mathbf{0}$, plus a solution of inhomogeneous equation [61]:

$$\mathbf{I}_b = \mathbf{M}^{\mathbf{T}}\mathbf{I}_s + \mathbf{D}\mathbf{I}_f \tag{7}$$

where $\mathbf{M}^{\mathbf{T}}$ is the transposed of matrix $\mathbf{M}$ which permit to write Eq.(5) in vector notation and $\mathbf{D}=\mathbf{R}^{\mathbf{T}}(\mathbf{R}\mathbf{R}^{\mathbf{T}})^{-1}$ with $\mathbf{R}^{\mathbf{T}}$ the transposed of matrix $\mathbf{R}$ carrying the effect of bias currents in the branches. This is the right way to include bias currents in the array rather than introduce them in a fictitious mode in Eq.(5). In the abridged derivation of the array equations sometimes the bias currents appears directly in the equations like above Eq.(5) which is correct at least for the leading terms in the bias currents. Now $\mathbf{I}_s$ can be derived from Eq.(7) thus obtaining:

$$\mathbf{I}_s = \left(\mathbf{L}\mathbf{M}^{\mathbf{T}}\right)^{-1}\mathbf{L}\mathbf{I}_b - \left(\mathbf{L}\mathbf{M}^{\mathbf{T}}\right)^{-1}\mathbf{L}\mathbf{D}\mathbf{I}_f \tag{8}$$

the term $\mathbf{L}\mathbf{I}_b$ can be derived now by Eq.(4) and Eq.(3), this give:

$$\frac{2p\,L_{mean}}{\Phi_0}\mathbf{I}_s = \left(\mathbf{L}\mathbf{M}^{\mathbf{T}}\right)^{-1}\left(\mathbf{M}\vec{j} - 2p\,\vec{f}_{ext} - 2p\,\vec{f}_{noise} + 2p\,\vec{n}\right) - \frac{2p\,L_{mean}}{\Phi_0}\left(\mathbf{L}\mathbf{M}^{\mathbf{T}}\right)^{-1}\mathbf{L}\mathbf{D}\mathbf{I}_f \tag{9}$$

inserting Eq.(9) in the Eq.(7) we found the following set equations:

$$\frac{2p\,L_{mean}}{\Phi_0}\mathbf{I}_b = \mathbf{M}^{\mathbf{T}}\left(\mathbf{L}\mathbf{M}^{\mathbf{T}}\right)^{-1}\left(\mathbf{M}\vec{j} - 2p\,\vec{f}_{ext} - 2p\,\vec{f}_{noise} + 2p\,\vec{n}\right) - \frac{2p\,L_{mean}}{\Phi_0}\left(\mathbf{M}^{\mathbf{T}}\left(\mathbf{L}\mathbf{M}^{\mathbf{T}}\right)^{-1}\mathbf{L} - \mathbf{1}\right)\mathbf{D}\mathbf{I}_f \tag{10}$$

normalizing all the currents appearing in this equation to the mean Josephson supercurrent I_{mean} in the JJA branches we can introduce the parameter $\beta_L=2\pi L_{mean}I_{mean}/\Phi_0$ which have an important role in determine the array behavior as we show below. We define the matrix $\mathbf{K}=\mathbf{M}^{\mathbf{T}}(\mathbf{L}\mathbf{M}^{\mathbf{T}})^{-1}$ and use the expression of branch currents given by RSJ model $\mathbf{I}_b = \ddot{\vec{j}} + \Gamma\dot{\vec{j}} + I_d \sin\vec{j}$ where Γ the normalized conductance of the Josephson element (here we assume that the point-like junctions have uniform properties in the array for dissipation and capacitance) and I_d is the normalized deviation of Josephson current from mean Josephson current; $\sin\vec{j}$ represents a vector which components are $\sin j_k$. Times in RSJ model equation are normalized to the (mean) plasma frequency of junctions, i.e., to $w_J=(2\pi I_{mean}/C\Phi_0)^{1/2}$. Now Eq.(10) can be rewritten as:

$$\ddot{\vec{j}} + \Gamma\dot{\vec{j}} + I_d \sin\vec{j} = \frac{1}{b_L}\mathbf{K}\left(\mathbf{M}\vec{j} - 2p\,\vec{f}_{ext} - 2p\,\vec{f}_{noise} + 2p\,\vec{n}\right) - \left(\mathbf{K}\mathbf{L} - \mathbf{1}\right)\mathbf{D}\mathbf{I}_f \tag{11}$$

This last set of equations gives just the $2N_c x N_r + N_r + N_c$ *explicit* equations for the phases. We remark that for other geometries the Eq.(11) is again valid but matrixes appearing in the equation are different. As can be view from Eq.(11) set the role of b_L is that of coupling coefficient between the phases of JJA junctions. In this sense "open arrays", i.e. arrays without coupling loops, are made of uncoupled junctions. Inductive coupling is only the most natural coupling for general 2D or 1D arrays when simulating magnetization properties, anyway sometimes other type of couplings are used (cf. ref.s [64] and references cited therein). In the limit of b_L goes to infinity the JJA is effectively made by uncoupled junctions. This happens from moderate until very large values of b_L depending on the type of problem under consideration: typically fast dynamical phenomena uncouple before static ones, so the first case will present at about b_L of the order of 10-100, cf. [62], the second toward b_L of the order of 1000 and larger. The limit for zero inductance is more complicate to treat because Eq.(2) become a constraint on the phases. This constraint is nothing but the condition of existence of a well-defined distribution of spin variables y on the superconducting islands of the model, i.e., the system reduce to XY model with $(N_c+1)x(N_r+1)$ sites. The phases are just the discrete derivative of spin field, so in the XY model they would be given by:

$$\vec{j} = \mathbf{R}^{\mathbf{T}}\vec{y} + \mathbf{M}^{\mathbf{T}}\left(\mathbf{M}\mathbf{M}^{\mathbf{T}}\right)^{-1}\vec{f} \tag{12}$$

where the second term account for the frustation effects (here we use a unique frustation $f=f_{ext}+f_{noise}$). Eq.(12) is a solution of Eq.(2) for zero self-induced flux because $\mathbf{M}\mathbf{R}^{\mathbf{T}}=\mathbf{0}$ [61]. Naturally the above Eq.(12) is true only in the limit of zero inductance, i.e., zero b_L when variables are reduced to node (site) number $(N_c+1)x(N_r+1)-1$, the other variables, i.e., the screening currents have been disappeared from equations (note that the last spin variable is actually an integration constant). In order to recover correctly this limit in presence of a finite b_L Eq.(12) must be generalized to [61]:

$$\vec{j} = \mathbf{R}^{\mathbf{T}}\vec{y} + \mathbf{M}^{\mathbf{T}}\left(\mathbf{M}\mathbf{M}^{\mathbf{T}}\right)^{-1}\vec{f} - b_L\left(\mathbf{Q}\mathbf{M}\mathbf{I}_s + \mathbf{Q}\mathbf{D}\mathbf{I}_f\right) \tag{13}$$

where $\mathbf{Q}=\mathbf{M}^{\mathrm{T}}(\mathbf{M}\mathbf{M}^{\mathrm{T}})^{-1}\mathbf{L}$. Here the branch coordinates are expressed as a sum of screening currents $\mathbf{I}_s$ and spin variables y (here called also "cut-phases" after [61]). Can be easily shown by direct substitution that Eq.(13) satisfy node, Eq.(3), and fluxoid quantization equations, Eq.(2). After substitution of Eq.(13) in branch current equations the dynamics is given by:

$$\ddot{\vec{y}} + \Gamma\dot{\vec{y}} = -\left(\mathbf{R}\mathbf{R}^{\mathbf{T}}\right)^{-1}\mathbf{R}\sin\left(\mathbf{R}^{\mathbf{T}}\vec{y} + \mathbf{M}^{\mathbf{T}}\left(\mathbf{M}\mathbf{M}^{\mathbf{T}}\right)^{-1}\vec{f} - b_L\left(\mathbf{Q}\mathbf{M}\mathbf{I}_s + \mathbf{Q}\mathbf{D}\mathbf{I}_f\right)\right) \tag{14a}$$

$$b_L\left(\ddot{\mathbf{I}}_s + \Gamma\dot{\mathbf{I}}_s\right) = -\left(\mathbf{P}\mathbf{P}^{\mathbf{T}}\right)^{-1}\mathbf{P}\sin\left(\mathbf{R}^{\mathbf{T}}\vec{y} + \mathbf{M}^{\mathbf{T}}\left(\mathbf{M}\mathbf{M}^{\mathbf{T}}\right)^{-1}\vec{f} - b_L\left(\mathbf{Q}\mathbf{M}\mathbf{I}_s + \mathbf{Q}\mathbf{D}\mathbf{I}_f\right)\right) - \left(\mathbf{P}\mathbf{P}^{\mathbf{T}}\right)^{-1}\mathbf{P}\mathbf{M}^{\mathbf{T}}\mathbf{I}_s \tag{14b}$$

where $\mathbf{P}^{\mathbf{T}}=\mathbf{Q}^{\mathbf{T}}\mathbf{M}^{\mathbf{T}}$. In these last equations the limit of zero b_L is harmful. When we take the limit Eq.(14a) decouple from Eq.(14b), i.e., the spin variables become independent from the screening currents. Moreover Eq.(14b) is nothing but the fluxoid quantization in the

form $\mathbf{M}\left(\ddot{j}+\Gamma\dot{j}\right)=0$ as follows by Eq.(2) with zero inductance. Historically the relation between XY model and JJA was introduced by Teitel and Jayaprakash and by Halsey [28]. The introduction of "cut phases" is just an example of how other gauges choices can be useful to treat the general JJA equations in cases where they are very stiff, so that a more standard strategy is unable to extract information from them. Description of gauge choices is found also in ref.[12].

The magnetic field enters in Eq.(11) via the frustation terms both with its mean value f_{ext} and fluctuation f_{noise}. We note that also if the mean field is uniform the contribution in each loop of the array in general not vanishes. In fact equivalent field currents, i.e. the term $\mathbf{K}f_{ext}$ in Eq.(11), have to generate the same field with different inductance between adjacent meshes, this implies that field currents cannot cancel in the common branch. Finally the last term is the effect of bias currents. These are propagated at the array nodes by matrix **D**, moreover an additional effect is found by the presence of **KL** matrix in the last term, this represents the mutual inductance induced flux by bias current circulation.

Explicit form of Eq.(11) permit direct integration, however would be said that it is rather heavy for large arrays, i.e., more than 30x30 meshes, because involve the use of a $o(N^4)$ components matrix **L** for an NxN array. So various methods have been devised for their integration, among these the most interesting are that reported in Phillips et al. [13], which use FFT to find an approximate solution of Eq.(4), a similar method is used by Dominguez and Josè [12]. Explicit integration of Eq.(11) was used by the authors in ref.s [62] where JJA are all below the 30x30 meshes, in this case explicit integration is practically equivalent to others methods in integration times (large differences, i.e., more that a factor 10, begin by about 50x50 arrays). A discussion of advantages of implicit or explicit routines is contained also in ref.[62]. Truncation of full inductance model can reduce time of integration by a large factor. Below we shown the NS-model [4] which requires only $o(N^2)$ integration times.

Naturally the above comments are valid if loop inductances and supercurrents do not differ too by that appears in the mean b_L (weak disorder assumption). If this does not happen arrays breaks in regions with very different magnetization and dynamical properties. This description, though is not convenient if many different scales are involved, can be interesting if only two scales are present or we are near the transition between two regimes. In this case this object will described as a superconductor made of "strong" Josephson type I regions, where b_L is larger than one, which presents many analogies with type I superconductors with a strong pinning of the field at the boundary (Meissner state) plus "weak" Josephson type II regions, in which b_L is less than one, in which Josephson vortex penetration is much easily and pinning forces weak. Critical state will be dominated by strong or weak properties depending on what is the prevailing regime. We try to give some results below for the simplest case of 1D arrays.

On this basis a rather delicate question is the relation between JJA and GL equations in view of above cited analogy between II type superconductors and Josephson systems. It is well known that the most intriguing difference between Abrikosov and Josephson vortices was in the fact that Josephson vortex has no normal core. More correctly Josephson vortex "core" is in the barrier, i.e., in the insulator, thus a minimal lattice space always remain in the Josephson case. Thus it is not surprising that can be easily proved that Eq.(11) in the linearized self-inductance model, i.e., when matrix **L** is equal to identity and $\sin j$ can be linearized to j, reduces to the London equation *on a lattice*. This means that the GL

equations itself for continuos superconductors [65] can be shown to be substantially equivalent to the self-inductance model for the arrays.

Here we do not suppose disorder affect the conductance Γ and the capacitance C appearing in the plasma frequency ω_J. This is rather obvious if we aspect that dissipation or charging effects are roughly constant over the HTC material we want simulate. Naturally this assumption can be released if necessary. Arrays can be classified as overdamped is $\Gamma>>1$, in this case the second derivative can be ignored and the system equations are written as a first order system of ODEs. If $\Gamma<1$ the array is underdamped and its junctions show hysteresis in their I-V characteristics. In this case the ODEs are second order in time and the number of variables is doubled. In general HTC materials have been described as overdamped systems, but in many problems they shows also hysteresis in the I-V characteristics which is a signature of underdamping (cf. for example ref.[66]). Moreover recent experiments on PME effect use underdamped arrays build on the basis of a comparison with HTC materials [58].

Another important factor is the ratio $E_J/\hbar w_J$ where E_J is the mean Josephson energy $I_{mean}\Phi_0/2p$. When the ratio is less than one the array is in the so-called quantum regime, i.e., the phase variable φ, which differences are related to the normalized magnetic flux, cannot longer be treated as "classical", so a full quantum treatment is necessary. This it is not taken generally in consideration in HTC materials especially in view of their typically large Josephson coupling, but in view of the new nanoscale applications this could not be true in the future.

In the Eq.(11) the flux noise term is a standard way to insert temperature dependence in the equations. This is necessary in all situations where temperature effects are important, among these we cite the thermal escape between static and dynamical situation and viceversa, the phenomena related to the flux creep, and the estimate of critical exponents. In all these cases the set of ODEs represented by Eq.(11) are stochastic Langevin equations and depends also on the property of the noise spectrum which needs careful modeling. In all other cases when mean Josephson energy are higher than the kT, i.e., when E_J/kT is much larger than one, the noise term is generally ignored. An exception can be given for situations in which randomness created by (thermal or external) flux noise is frozen out by a successive growth of the Josephson energy. In this case the problem of the noise description is just in the choice of random initial conditions, we will describe one of this case below. Naturally (external) flux noise it is not the only noise term in Eq.(11), another noise term can be due to the conductance Γ, i.e., the thermal noise due to shunt resistor in RSJ model, in principle both contribute to phase fluctuations, but their effects can be different: large flux noise, i.e., with $f_{noise}>1$, is linked to phase-slips in the array, whereas the thermal noise is linked to plasma oscillations (phonons). These two types of noise have a different behavior in temperature [67].

Finally it is important to note that JJAs based on Josephson coupling between different island or crystal made of homogeneous HTC material are probably not the only model possible for granular HTC superconductor. A GL based approach for HTC superconductors is used by Davidovic and Grujic [68]. Another non-circuital model is the so-called Time Dependent Ginzburg-Landau (TDGL) model which was used by Tiesinga et al. [69] to study the flux noise near the BKT transition in the XY model and compare it with circuital RSJ model in the zero inductance limit which, as we shown above, is just another form of XY Hamiltonian. Comparison with experiments seems rule out the RSJ

model in favor of simplest TDGL. A different non-circuital model is the ab initio molecular dynamics pinning model of Reichhardt et al. [38] where vortices propagate in a regular array of pinning centers with the standard bulk forces based on the London equation. The behavior of this model is in some respect different from circuital JJA. Recently also in high frequency oscillators based on LTC-JJA the circuital model of JJA was questioned (see P.Barbara et al. in ref.[5]).

3.STRONG TO WEAK PINNING TRANSITION IN 1D ARRAYS

3.1 1D JJA for the analysis of flux penetration between GBs.

In the 1D JJA if we assume that only self-inductance loops contribute in the fluxes Eq.s (3) we have $\mathbf{L}=½\mathbf{M}$ from which we have $\mathbf{K}=\mathbf{M}^{\mathrm{T}}$. If we note that we have only two junctions per loop then $\mathbf{M}$ itself reduces to difference operator Δ between adjacent meshes. Finally $\mathbf{D=1}$ because the number of nodes equals the number of branches containing junctions. Eq.(11) becomes:

$$\ddot{\vec{j}} + G\dot{\vec{j}} + I_d \sin \vec{j} = \frac{1}{b_L}\Delta\left(\frac{\Delta\vec{j} - 2p\ \vec{f}_{ext} - 2p\ \vec{f}_{noise} + 2p\ \vec{n}}{L_d}\right) + \mathbf{I}_f \qquad (15)$$

this is a set of $N=\mathrm{N_c}+1$ ($\mathrm{N_r}=1$) equations in which L_d is the normalized deviation from mean inductance of the loops. In Eq.(15) disorder can appears in both currents and inductances via the terms I_d and L_d. We note that also with the simple assumption of ignoring mutual inductance the general equations do not reduces to Sine-Gordon model. Can be shown that if we use next-neighbor approximation in the inductance matrix 1D JJA can be also well-described by the same models reported above by substituting L with $L-2M$ where the factor two depends on the number of the next-neighbor meshes [70]. This is especially true when values of b_{L} are not very large. An upper limit for this is in the interval 4-8 depending on the specific mutual inductance model. Only if we assume that all loops have *equal* self-inductances we can set L_d equal to 1 so Eq.(15) becomes:

$$\ddot{\vec{j}} + G\dot{\vec{j}} + I_d \sin \vec{j} = \frac{\Delta^2\vec{j}}{b_L} - \frac{2p}{b_L}\Delta\left(\vec{f}_{ext} + \vec{f}_{noise} - \vec{n}\right) + \mathbf{I}_f \qquad (16)$$

that is the Discrete Sine-Gordon equation (DSG) similar to that appearing in ref. [8]. We note that is external field is uniform the term with frustation f_{ext} is absent except to the boundary meshes of the array where field terms do not cancel. So for geometrically similar loops the field penetrate the array only via its boundaries, or to say in a different manner, the array naturally screen any uniform magnetic field. The same is not true for flux noise f_{noise} or a distribution of cooling remnant flux quanta that can given by a random vector of n. If we pose $b_L=\Delta x^2/l_{\mathrm{J}}^2$ where Δx is the lattice space, l_{J} is a physical distance and taking the limit for Δx goes to zero Eq.(16) become SG equation used in the study of LJJ. Frustation terms transforms in normalized boundary magnetic field h writing them as $f=h\Delta$x. Inverting the relation between b_L and Δx we obtain the definition of Josephson

penetration length: $l_J = \sqrt{\frac{\Phi_0}{2p\ J_0 \ell_0}}$ where $J_0=I_{mean}/\Delta x$ is the mean critical supercurrent density and $\ell_0 = L_{mean}/\Delta x$ is the mean inductance per unit length. If we define the normalized length of the junction $l=L/l_J$ then the relation between l and b_L is $l=Nb_L^{1/2}$ where N is the number of sections in which we divide the junction. This relation is the link between continuos and discrete SG: for a given l the equivalent N-JJA can be written with the b_L given by this relation. This is the standard way in which SG is solved numerically by finite difference method in particular for dynamical phenomena where sta tic method are unable to work. In numerical simulation only for the smallest values of b_L the behavior will be essentially the same, otherwise the system will be discrete, in particular it will be discrete for b_L larger than one. Note that in strongly discrete 1D JJA the "formal" Josephson length as derived by $l_J=\Delta x/b_L^{1/2}$ is typically smaller than JJA lattice dimension, being b_L larger than one. This means that any array loop can easily accommodate more than a flux quantum.

We note that the SG continuos limit is essentially driven by boundary conditions, especially if junctions are uniform the only way to drive LJJ is via boundary conditions which, depending on the geometry and symmetry, assume the form of currents or magnetic fields. On the other hand discrete 1D JJA equation use loop fluxes in a way more similar to SQUIDs to couple the system to external field and an independent vector of bias currents.

In DSG we can again have a Josephson supercurrent dependent on array index (or, which is the same, the spatial variable in SG). The current can vary periodically or be randomly distributed. Both cases in the SG limit are treated in ref.[9]. What we want to stress is that in SG limit periodic modulation of supercurrents can give strong pinning only for some values of external field because in the continue limit the vortex lattice spacing is dependent on the field itself.

Anyway the general model given above, Eq.(15), it is not restricted to supercurrent variations. Another interesting model is that in which we have a periodicity in the loop inductance that could be imposed also over a weak disorder in the currents. In this case the equations are similar to Eq.(15) with the exceptions that L_δ now is a periodic function over the array lattice with a period $n<N$, we refers to this as "periodic model" (cf. Fig.1c where n=2 and n=4 periods are shown). This can be useful to represents purely "geometric" characteristics as regular meandering of GB, that can be described as a periodic variation of the geometry along the percolative path between GBs. We stress that this model cannot be described by pure SG model. In fact in the above Eq.(15) disorder or periodic model for L_d implies that the pinning properties are different from simplest DSG. Mainly is the nature of field penetration is very different in Eq.(15) respect to DSG: in this last model penetration of the field happens exclusively at the sample boundary whereas in general for both disordered or periodic L_d field penetrate the whole arrays depending on inductance variations because frustation factors *do not* cancel out in the second member of Eq.(9) also if the external field is very uniform. Moreover the difference operators *do not* reduce to DSG case if inductances are different. Naturally if loops become very small any variation of inductance can be made sufficiently small to approximate SG model, thus this difference is relevant for discrete systems only.

These considerations can apply in principle also to 2D array. The extension of these models in 2D arrays will be useful to describe cases in which the JJA simulate an HTC

materials made of regions with different magnetization properties: strong regions will show Meissner effect whereas weak region will be penetrated by the field. Anyway response in 2D case is more complex, as we show below for the PME, because of 2D nature of vortex-vortex interaction which give arise to a not trivial magnetic behavior also in absence of disorder. So we limit here to simplest 1D case.

What we want describe here is just the transition between continuos and discrete cases. This is interesting because pure not disordered continuos limit LJJ do not show pinning except at the boundaries. Long uniform junctions pin weakly than shortest because flux quanta can easily propagate along the junction because there are no energy barrier being the system traslationally invariant. To pin in continuum we need defect and so a disordered model [9]. Anyway disordered LJJ pins again, generally speaking, in "weak" sense because flux quanta cannot be squeezed too much in the continuos case, so they can overcome barriers created by defects simply because there is no space to put another vortex. Only for particular values of field and for determined, e.g., periodic, distribution of defects, the critical current is higher due to the commensurability between defects and vortex lattice periods. But these states cannot survive at a different field value because in the continuum vortex spacing is determined by the field. On the other hand in discrete JJA pinning barriers can be very strong because large b_L implies uncoupled point-like junctions that can show a very high critical field. Naturally we have to distinguish the critical field of single small junctions H_s by the system critical field H_g that is generally lesser than H_s.

A study of transition between discrete pinning and continuous pinning could be useful to describe the pinning properties of the GB for different misorientation angles. For small angles the GB can be considered the analogue of a strong pinning system as a high b_L array, at larger angles regions of weak pinning, i.e., the so-called Josephson channels [42], begins to appear. For the largest angles the system is totally weak-pinning dominated. It is interesting to note that also the difference between bulk and film critical currents [37] could be explained in analogous way: more regular bulk crystals shown weak pinning with respect to meandering film crystals. Roughly translated in JJA language this means that bulk behavior have mean b_L under one, whereas films have mean b_L larger than one or, more probably, regions of higher b_L which separate more-less LJJ regions. It is worth to remember that the possibility of discrete small junctions behavior it is invoked also in the case of large angle thin films, but the data can be reinterpreted and compared with bulk using a qualitative theory of pinning strength in LJJ [37]. On the other hand we note that "strong" channels in HTC materials are most likely assumed to be GL described rather than Josephson. This means that Josephson vortices can be thought as merging almost continually with Abrikosov vortices pinned on the side of percolative path (cf. [37]). Anyway just "strong" channels, in Josephson sense, can pin Josephson vortices at their boundary which behavior it is not much more different than Abrikosov vortices. In "weak" channels these same vortices can much more easily move anticipating the set up of the critical state. Finally we note that it is possible to consider also other models, somewhat similar to the distribution of defect radii in LJJ of ref.[9]. This is the possibility of have, along the array, a distribution of "weak" and "strong" pinning regions with different lengths. This is also a view similar to ref.[46] in which a distribution of Junction lengths is introduced along the array (though these are practically uncoupled junctions). The effect of this length disorder can be linked to the changing the period n on which the magnetization properties vary.

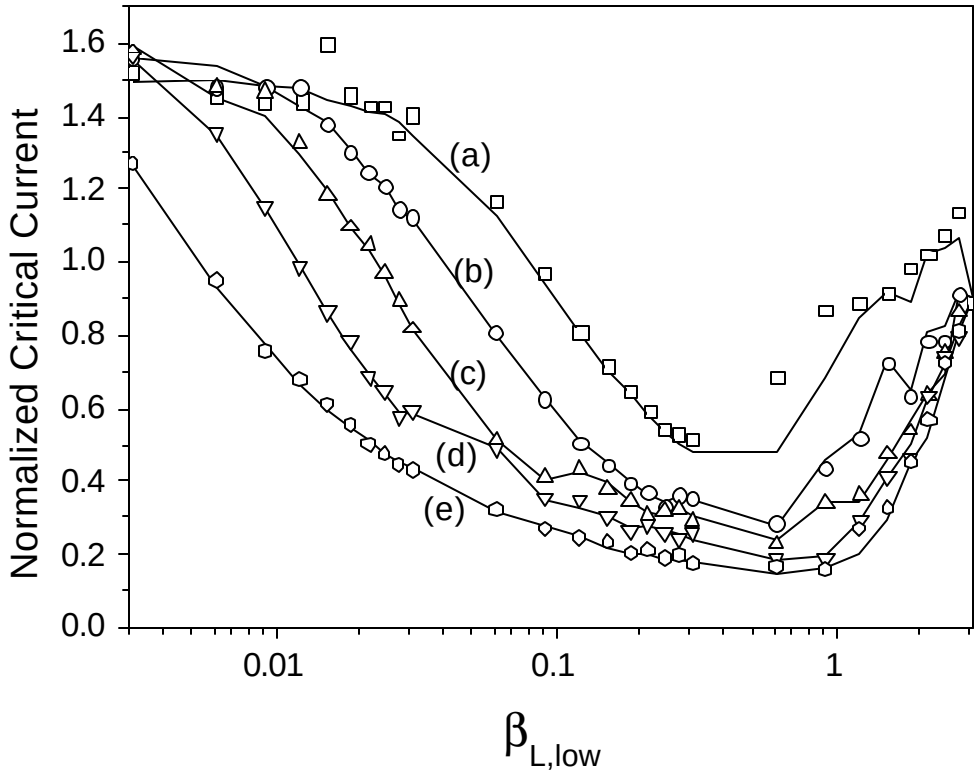

Fig.2 Critical current for an N=48 JJ 1D array with periodic variation of inductance along the array. On the x-axis is the inductance variation over the chosen period measured by the lower value of b_L, i.e., $b_{L,low}$. The maximum $b_{L,max}$ is fixed to 3.06. In all plots continuos line is the disorder free critical current, scattered points represent different realizations of the array with weak disorder in the supercurrents with a spread of 25%. (a) Periodic array with n=2; (b) periodic n=4 array; (c) periodic n=8 array; (d) periodic n=16 array, (e) uniform system with only one $b_L = b_{L,low}$.

3.2 Numerical results and discussion

We simulate the making of critical state in a 1D array made of N junctions. b_L was chosen to vary periodically along the array with a period n+1 (cf. Fig.1c). Discrete regions was supposed to be made by a single mesh of the array, whereas the other n meshes have a lower b_L. Array was biased in so-called asymmetrical inline geometry, this permit comparison with both theory for LJJ in ref.[9] and also with experiments where largest screening currents circulate to the edge of the sample. Thus the other edge of the array is roughly the corresponding of the sample center in this geometry (or is a strongest pinning region where flux cannot penetrate). Following [48] we call "active" edge the side of the junction where the current is feed. In the simulations frustation is related to the normalized magnetic field by the relation: $f = hDx = hb_L^{1/2}$. The critical state was determined dynamically sweeping the current until a switch to resistive state was observed. In order to

make a precise evaluation of criticality we note that the signal of resistive switch is given by the full penetration of the field in the array. This means that there is no critical state, but only flux redistribution over the array, until the last not-feed junction of the array begin to sense the field which penetrate in the last mesh. It is worth to point out that we treat discrete arrays, not continuos junctions, so the magnetization and pinning properties described here are different from that of ref.[9], also if some similarity appears as we shown below. This is due to the fact that both cases treat with inhomogeneity and this can alter the pinning properties.

We report in Fig.2 the normalized zero field critical current as function of lower value of $b_{L,low}$ for an array with N=48 junctions and with maximum $b_{L,max}$=3.06. Current is normalized to the half of the total supercurrent $\frac{1}{2}NI_{mean}$ so the maximum normalized current is 2 as is usual for inline geometry. The zero field critical currents is interesting for the measurement of self-field effects itself, i.e., effect generated by feeding current alone, and it gives a measure of the zero-field pinning strength of the array. Lower values of $b_{L,low}$ range from 90% to 0.001% of $b_{L,max}$, so the array behavior is crossing the whole region between discrete system to continuos junctions. In the small $b_{L,low}$ limit due to remaining meshes with high b_L the array will break in a series array of LJJ. The behavior of an homogeneous array in which n is larger than array length, so there is only a value of b_L for the whole array is reported by comparison in the curve (e). In zero magnetic field for a homogeneous system in both limits of large or small b_L the critical current is large. First maximum on the right of Fig.2 is due to pure discrete array, which magnetizes following the Bean model of field penetration, we call it the Bean peak. Pre-critical magnetic flux and supercurrents distribution over the Bean peak is reported in Fig.3a: the flux profile is just linear as in Bean model, in the critical state the Bean staircase extends until the passive end. The regular supercurrent distribution between sections 15-40 is a commensurability pattern similar to that reported in ref.[8]. The maximum on the left in Fig.2 for small values of $b_{L,low}$ is due to Meissner effect in the long junction formed for $b_{L,low}$ which goes to zero, so the left peak is actually the well-known Meissner peak in continuos systems. The pre-critical flux profile in Fig.3b show a (weak) localization of the field at the active edge of the junction. We note the great scale difference between the previous case: flux is less the 1/10 of a flux quantum at the active end. Field is strongly expulsed by the array that is similar to a long junction. The same considerations apply to the supercurrent profile that is reported again in the Fig.3b. The limiting value of the critical current is just corresponding to a junction of normalized length 2.65 which is found with above relation between b_L and Δx, this give a limit of about 1.3 for the zero field critical current in the long junction continuos limit. Bean and Meissner peaks correspond to very different dynamics of field penetration in the array: Bean-like penetration fills the array with flux quanta until this becomes critical. On the other hand Meissner expulsion of flux, though having a strongest pinning, as it is evident from the largest critical current in zero field, cannot permit penetration of flux quanta until critical state itself, i.e., the only field in Meissner state is found at the junction edges [9]. Between the two peaks there is a strong depression of critical current until about 1/7 of its maximum value on the Meissner peak, this region corresponds to $b_{L,low}$ about equal 1/5 to 1/10 of $b_{L,max}$. It is important to note that the above distinction between Bean and Meissner peaks is functional to our discussion of Fig.2. The two distinct behaviors can be however co-exist as is shown in ref.[9] when the case of “optimized” junctions is treated, or as we shown below where a

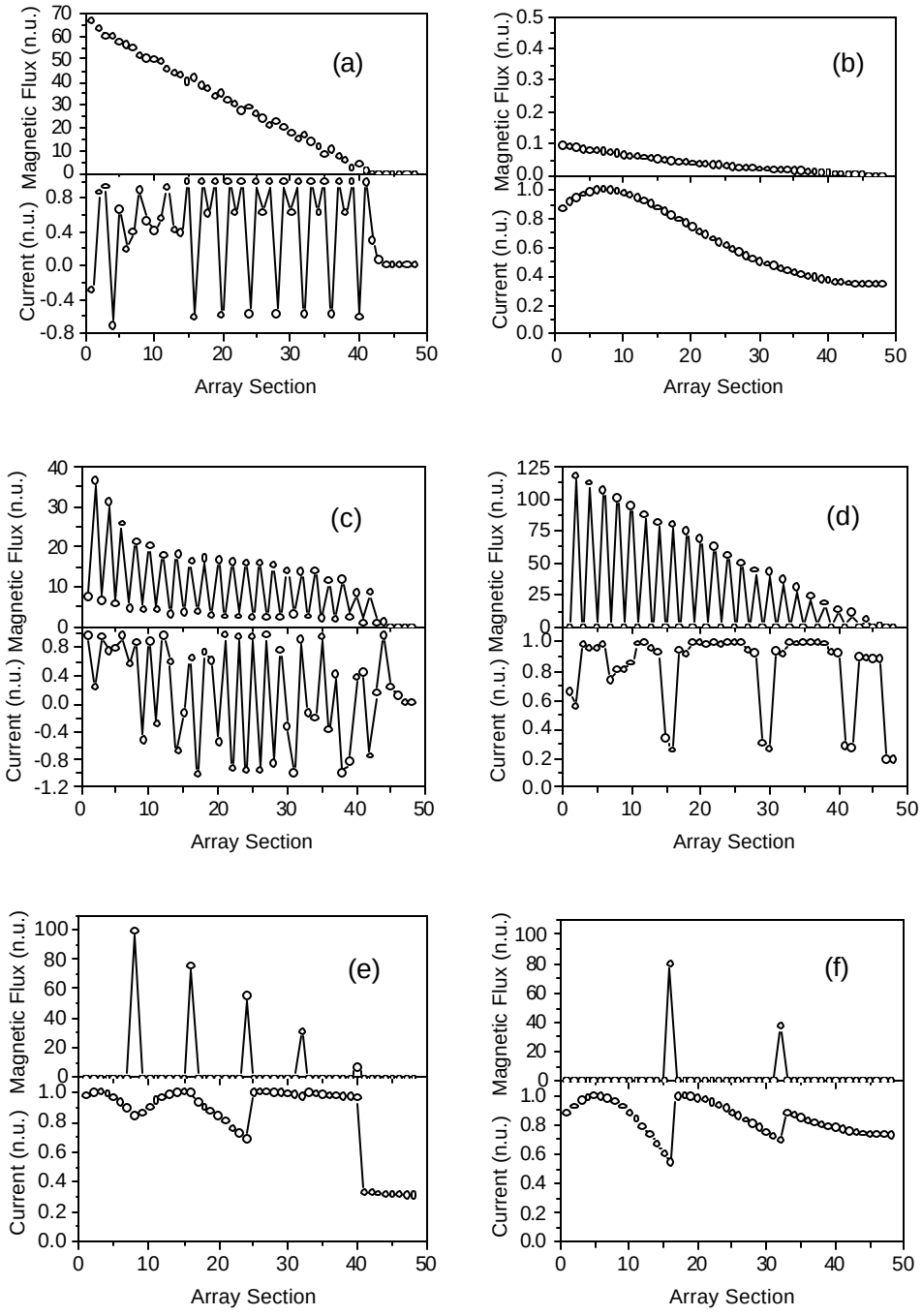

Fig.3 Precritical internal profiles of magnetic flux (top) and supercurrents (down) for N=48 JJ 1D array in zero magnetic field, active edge is on the left, fluxes are normalized to flux quantum Φ_0 and currents to maximum supercurrent for section. (a) Uniform array with $b_{L,low}=b_{L,max}$; (b) uniform array with $b_{L,low}=0.00306$; (c) periodic array with n=2 and $b_{L,low}=b_{L,max}/5=0.612$; (d) periodic array with n=2 and $b_{L,low}=b_{L,max}/1000$; (e) periodic array with n=8 and $b_{L,low}=b_{L,max}/1000$; (f) periodic array with n=16 and $b_{L,low}=b_{L,max}/1000$.

similar coexistence can be obtained in a discrete system made of small continuos junctions. For n<N the behavior is more complex being a mixture of both Bean penetration and Meissner side-pinning expulsion, anyway the curves continue to shown two distinct peaks. Curve (a) in Fig.2 is traced for n=2, i.e., the shortest period, the array is equivalent to a chain of coupled dc-SQUIDs. As general comment the effect of this inhomogeneity make the critical current everywhere larger. In the intermediate coupling depression is weak in n=2 array, thus the short period is making the array shown again stronger pinning properties also in the region of current depression. A plot of internal magnetic field and supercurrent is shown in Fig.3c. There is a large number of flux quanta distributed over the array, but they are placed mainly at the loops where b_L is large, in the low b_L loops there is a partial expulsion. This phenomenon is enhanced near the Meissner peaks: the system now presents clearly a chain of mixed Bean-Meissner regions. Here the array is well represented by an array of very small junctions (not point-like however). This can be viewed looking at the precritical field profile and supercurrent distribution which is shown in Fig.3d: the envelope of flux profile is again Bean-like, but flux is almost totally expulsed by loops with $b_L = b_{L,low}$, i.e., in the small junction limit. Supercurrent distribution shows a higher mean value respect to previous cases. Higher critical current in this region derives by the fact that the required Bean-like distribution of flux quanta necessary to obtain the critical state have to cope with Meissner regions represented by low b_L regions that act as stronger pinning centers confining the field at their boundaries.

The other curves (b), (c) and (d) in Fig.2 show respectively n=4, n=8 and n=16 cases. In general the behavior of these arrays is intermediate between homogeneous case and n=2 case. Moreover current depression at intermediate $b_{L,low}$ is larger than case n=2 reaching roughly the same ratios of homogeneous system. On the other hand the Meissner peak is larger than homogeneous system suggesting that inhomogeneity is changing the pinning properties of system as in the case of n=2. The maximal critical currents on the left is reached for n=8. Other field profiles and supercurrents are shown in Fig.3e,f for the cases of n=8 and n=16. We observe how the Meissner field expulsion in the low b_L increase with the increase of n passing from n=2 to n=16. On the other hand these regions are weakening for the pinning because the high b_L regions are reduced in number and within low b_L regions barriers are absent (or small with current disorder). The maximal difference in the critical currents in Fig.2 is about 1/9. This number is however dependent on N and on the maximal $b_{L,max}$. For large N and $b_{L,max}$ this ratio generally increase. Here we stress that *without* using a very large value, i.e., just 3.0635, the difference in the critical currents and fields is roughly of one order of magnitude. Moreover for large N the critical current tend to increase because the field have to penetrate in a longer array. In Fig.2 the scattered points represents the effect of adding a weak disorder on the supercurrents alone with a spread of the 25%. Each point represents a different realization. Disorder do not alter the general behavior, only in the case of n=2 it seems increase further the critical current for some points.

In Fig.4 we show the behavior in magnetic field for some of the cases of Fig.2. Magnetic field is in general imposed at both the extrema of the array (symmetric magnetic field boundary conditions, SMF), because it really penetrates the whole geometry when differences in b_L between the adjacent loops are significant. Anyway also another possibility is considered in which the field is present only at the active end and an open boundary condition is set at the passive end (asymmetric magnetic field boundary

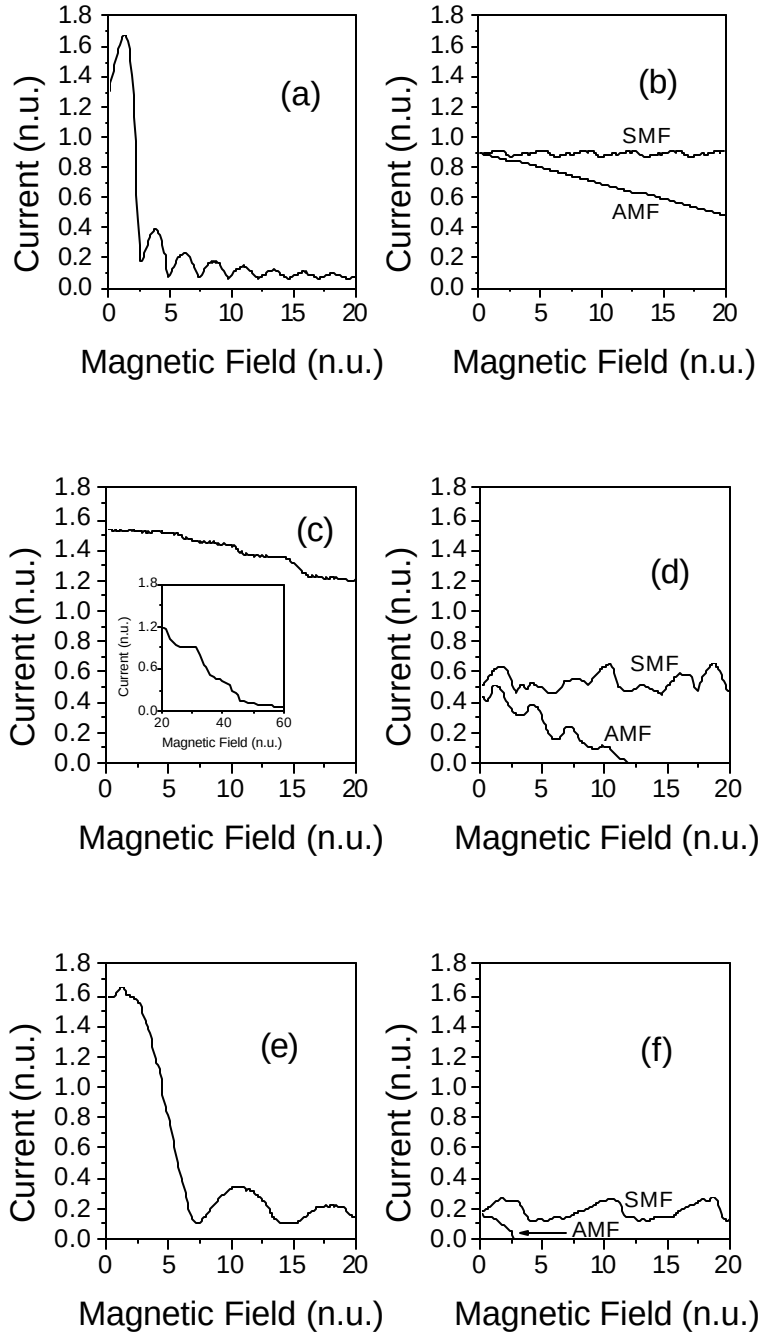

Fig.4 Magnetic field behavior of an N=48 JJ 1D array. SMF label the symmetric boundary condition case and AMF the asymmetric one, where label not appears SMF is the default. (a) Uniform array with $b_{L,low}$=0.00306; (b) uniform array with $b_{L,low}=b_{L,max}$; (c) periodic array with n=2 and $b_{L,low}$=0.00306; (d) periodic array with n=2 and $b_{L,low}=b_{L,max}/5$=0.612; (e) periodic array with n=16 and $b_{L,low}$=0.00306; (f) periodic array with n=16 and $b_{L,low}=b_{L,max}/5$=0.612.

conditions, AMF). This corresponding to a no field on one side of array, as region to be again penetrated by the field or a closed "strong" region. It is worth to stress that the choice of boundary conditions is critical to the array behavior especially in the discrete case, so this alternative will be considered in the discrete, i.e., large $b_{L,low}$, cases reported here. In AMF the sign of the field is chosen in order to favor the flux penetration, in symmetric case the sign do not alter the gross behavior except for the presence of the Meissner peak in the magnetic field patterns. Beginning with the homogeneous system for the minimum $b_{L,low}$ in Fig.4a that presents a typical asymmetrical "inline" junction pattern with a rapid decrease of critical current after the Meissner peak. The field at which the first flux quantum penetrate in the junction is known as H_{c1}, in this case after the first penetration of flux in the junction it can be easily put it in the resistive state because flux quanta move without difficulty in the junctions. The precritical profiles in Fig.5a show the so-called vortex lattice solution. The case of homogeneous discrete system is presented in Fig.4b; here for SMF case there is only a long plateau. The plateau is actually infinite because for this geometry to more flux in entering in the array on the active end, the same flux is entering on the other end of the array, as can be viewed by precritical profiles reported in Fig.5b. Here two commensurability patterns are evident around the section 40. The infinite plateau is due to point-like junctions, i.e., these cannot sense the field. The AMF is shown on the same figure and give a linear decrease (this is exactly true for homogeneous system where asymmetric b.c. are equivalent to an added boundary current) of the critical current according to: $I=I_{max}-a\eta$ with a roughly equal to one. When junctions are not point-like the result is shown in Fig.4c for a n=2 array with $b_{L,low}$=0.00306: the plateau continue until the "small" junctions forming the arrays reach their critical field as show in the inset (actually this relatively large field is lower than small junctions limit $2\pi/l$, which is valid for small junctions, because of rather crude n=2 assumption). The profiles reported in Fig.5c show how the array is penetrated by flux in large b_L loops where the "small" junctions regions contain less than a flux quantum. It is also evident that Bean penetration is again interwoven with Meissner expulsion. Increase of the period n until 16 have the effect of reducing the critical field until a factor compatible with continuos junction theoretical length that will be about 0.9 in this case. As is reported in Fig.4e for the same $b_{L,low}$=0.00306, here critical field is just given by $2\pi/l=2\pi/0.9=2\pi(3/2.65)$ where the factor 3 is due to 48/16=3 junctions in which the homogeneous case is broken. The precritical profiles, reported in Fig.5d, show confinement of the flux in the remaining large b_L loops. Magnetic behavior for intermediate values of $b_{L,low}$ is reported in Fig.s 4d,f . In the case of SMF b.c. a periodic pattern without apparent critical field appears similar to homogeneous point-like case of Fig.4b. Ripples in the critical currents are due to commensurability of flux quanta distribution with array lattice. For AMF b.c. a critical state is rapidly reached especially for the long period n=16. The precritical profiles are similar to homogeneous discrete case of Fig.5b. Current disorder was not shown in Fig.4, but we have tested that its effect is not dissimilar from that just viewed in Fig.2 where points follow roughly the disorder free curve. The main effect of disorder is to smooth the various ripples observed in the magnetic field behavior.

As general comments we can say that both discrete JJA with AMF and point-like junctions or discrete JJA made of short junctions show large critical currents and field (case b and c in Fig.4). The AMF boundary conditions seems describe in any case a roughly linear decrease of the critical current similar to single bicrystals [42] whereas SMF b.c. for a

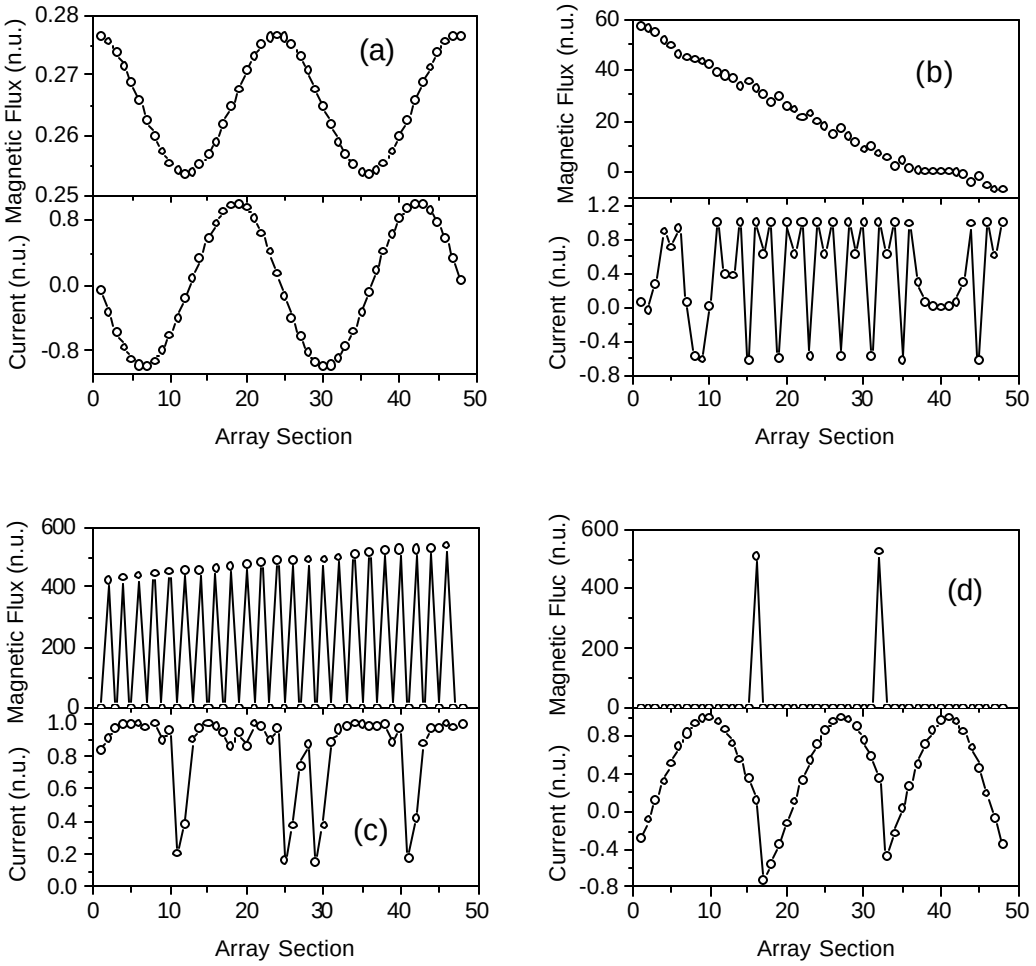

Fig.5 Precritical internal profiles of magnetic field and supercurrents for N=48 JJ 1D array in non-zero magnetic field fluxes are normalized to flux quantum Φ_0 and currents to maximum supercurrent for section. (a) Uniform array with $b_{L,low}$=0.00306 and η=5; (b) uniform array with $b_{L,low}=b_{L,max}$ and η=5; (c) periodic array with n=2, $b_{L,low}$=0.00306 and η=5; (d) periodic array with n=16, $b_{L,low}$=0.00306 and η=5.

short junctions JJA shows a behavior much more similar to the films reported in [46]. Best pinning properties thus are associate to a combination of discreteness and Meissner pinning at the boundary. Moreover shortest junction give the strongest pinning. This can justify the larger critical fields observed when the sample is irradiated to create random artificial columnar defects in it [46]: defects simply contribute to the shortening of junctions that are present in the sample.

4.FIELD COOLED 2D ARRAYS

4.1 2D model for PME effect in LTC JJA.

Here we change the approach with respect to 1D case: we prefer use full mutual inductance model but in order to compare with PME experiments on LTC arrays we have to study much more ordered arrays. This means that all the loop self-inductances and supercurrents can be chosen equal, moreover also mutual inductances for corresponding branches will be equal so $L_{mean}=L$ and $L_d=1$, $I_\delta=1$. Than we make the following modification to the Eq.(11) to put it in a form more appropriate for study the Field Cooling (FC) process: i) first we multiply Eq.(11) by $b_L/2\pi$; ii) the term $b_L/2\pi$ in front of second time derivative can be combined with plasma frequency normalization giving a new normalization which is simply $1/(LC)^{-1/2}$ which is the loop resonance frequency, it is important to note that this term is independent by Josephson supercurrents; iii) the term $b_L G/2\pi$ can be also combined with plasma frequency, using the new time normalization it becomes equal to $(b_L/b_C)^{-1/2}$ where $b_C=1/\Gamma^2$ is the Stewart-McCumber dissipation parameter; iv) field cooled JJA for the study of PME are not biased so there is no bias current term in the equation. After this Eq.(11) reads:

$$\ddot{\vec{j}} + \sqrt{\frac{b_L}{b_C}}\dot{\vec{j}} + \frac{b_L}{2p}\sin\vec{j} = \frac{1}{2p}\mathbf{K}\left(\mathbf{M}\vec{j} - 2p\ \vec{f}_{ext} - 2p\ \vec{f}_{noise} + 2p\ \vec{n}\right) \qquad (17)$$

We give here some important properties of Eq.(17) for 2D arrays beginning with next-neighbor case. In principle self inductance model will implies that $\mathbf{L}=¼\mathbf{M}$ that is analogue to 1D case. The factor ¼ is just accounting for branch inductance remembering that **L** is the branch-loop mutual inductance matrix. Anyway this model it is not really much used, because a next-neighbor model for 2D gives a simplest equation. To derive this we assume that mutual inductance matrix **L** reduces to blocks of the type:

$$\tfrac{1}{4}\begin{pmatrix} -1 & 0 & 1 & -1 & -1 & 1 & 0 \\ 0 & -1 & 1 & 1 & -1 & 0 & 1 \end{pmatrix}$$

which represents two adjacent meshes with their seven branches that carry simple next-neighbor interactions in the elements not common to the oriented mesh sum, i.e., elements a_{23} and a_{15} which are the branches parallel to central common branch indexed by column index 4 (other column, 1,2 and 6,7 are the four orthogonal horizontal branches which do not contribute to mutual induction at common branch). Then the square matrix **KM** becomes (here we give the results for two adjacent meshes, equivalently can be said that $\mathbf{K}=\mathbf{M}^{\mathbf{T}}$, i.e., formally this is similar to 1D self inductance case):

$$\mathbf{KM} \equiv \mathbf{M}^{\mathrm{T}}\mathbf{M} = \begin{pmatrix} 1 & 0 & -1 & 1 & 0 & -1 & 0 \\ 0 & 1 & 0 & -1 & 1 & 0 & -1 \\ -1 & 0 & 1 & -1 & 0 & 1 & 0 \\ 1 & -1 & -1 & 2 & -1 & -1 & 1 \\ 0 & 1 & 0 & -1 & 1 & 0 & -1 \\ -1 & 0 & 1 & -1 & 0 & 1 & 0 \\ 0 & -1 & 0 & 1 & -1 & 0 & 1 \end{pmatrix} \tag{18}$$

this means that this model involves only the phases of two loops having the common branch as in ref.s [10]-[11] (note that the center of matrix in Eq.(18) is just the Δ^2 operator appearing in the DSG equation Eq.(16)). Then Eq.(17) becomes:

$$\ddot{\vec{j}} + \sqrt{\frac{b_L}{b_C}}\dot{\vec{j}} + \frac{b_L}{2p}\sin\vec{j} = \frac{1}{2p}\mathbf{M}^{\mathrm{T}}\left(\mathbf{M}\vec{j} - 2p\ \vec{f}_{ext} - 2p\ \vec{f}_{noise} + 2p\ \vec{n}\right) \tag{19}$$

historically this was the first 2D-model equation derived in 1981 by Nakajima and Sawada [4]. Note that NS model it is not only self-inductance, but rather it represents the next-neighbor model for 2D arrays. This reduction from Eq.(17) to NS equations is a noteworthy property of 2D JJA equations that have no analogue in 1D case. NS equations are roughly o(N^2) in the integration time because a given phase depends only by its six neighbor phases.

A further improvement can be made on Eq.(19) if we use an effective value for the self-inductance which now is L_{eff}=L-4M due to four next-neighbor meshes (cf. ref. [12]), this accounts also for the six meshes surrounding the above two adjacent meshes. More generally will be possible to use truncated matrixes rather than full matrix, but as shown in ref. [62] the order of truncation have to be relatively large because at least 50% of the array dimension have to be included in order to give significant results. This agree with ref.[13] where only matrix elements less than 10^{-3} was truncated. It means that there is no effective advantage to use truncated models rather than full matrix. Among the advantages of full matrix approach is that the current profiles toward the array center for approximate models are unavoidably wrong for truncated approaches (cf. the excellent discussion in the appendix of Dominguez and José [12]), this implies that in 2D case the correct current distribution is obtained only with full matrix approach.

To evaluate the full mutual inductance matrix we use the following expression of mutual inductance between two vertical branches in the array which are *Ia* coordinates apart along x and *Ja* coordinates apart along y, where *a* is the mesh dimension [62]:

$$M^{b}_{I,J} = \int_0^a dy \int_0^a dy' \frac{1}{\sqrt{(y - y' + Ja)^2 + (Ia)^2}} \tag{20a}$$

this approximation is thin-wire actually, i.e., distant branches are treated as wires. It can be improved simply changing the integration extrema to account the “wire spaces” in the

mesh, but do not change significantly the results except when the ratio between wire section and mesh is larger than 0.25. Integration in (20) gives:

$$M^{b}_{I,J} = \frac{m_0 a}{4p}\left[F(J+1,I) - 2F(J,I) + F(J-1,I)\right]$$
$$\text{with} \qquad F(J,I) = \sqrt{J^2+I^2} + \sinh^{-1}\left(\frac{J-\sqrt{J^2+I^2}}{I}\right) \tag{20b}$$

for the mutual inductances of the horizontal branches the formula is the same with I and J interchanged. For $I=J=0$ the above formula cannot be used because we have to evaluate the self-inductance of the square mesh, we use [62]:

$$L = \frac{2m_0\, a}{p}\left[1.15\ln\left(\frac{a/r+0.096}{a/r}\right)+1.96\right] \tag{20c}$$

where r is the film dimension. Now we return to Eq.(17) to derive an expression for the magnetization. If we write the normalized total flux for a single mesh, cf. Eq.(2), as:

$$\frac{\vec{f}_{tot}}{\Phi_0} = \frac{1}{2p}\left(\mathbf{M}\vec{j} + 2p\,\vec{n}\right) \tag{21}$$

from static Eq.(17) we obtain that in absence of screening (super)-currents the total flux is equal to external flux. Combining Eq.(21) with external flux we have the mesh magnetization:

$$\vec{m} = \frac{\vec{f}_{tot}}{\Phi_0} - \frac{\vec{f}_{ext}}{\Phi_0} = \frac{1}{2p}\left(\mathbf{M}\vec{j} - 2p\;\vec{f}_{ext} - 2p\;\vec{f}_{noise} + 2p\;\vec{n}\right) \tag{22}$$

This implies also that Eq.(17) can be written as:

$$\ddot{\vec{j}} + \sqrt{\frac{b_L}{b_C}}\dot{\vec{j}} + \frac{b_L}{2p}\sin\vec{j} = \frac{1}{2p}\mathbf{K}\vec{m} \tag{23}$$

Analogous relations are valid for the averages of flux and magnetization of the array that can be written as:

$$\left\langle\frac{\vec{f}_{tot}}{\Phi_0}\right\rangle = \frac{1}{2p}\frac{1}{N_{loops}}\sum_{loops}\left(\mathbf{M}\vec{j} + 2p\,\vec{n}\right) \tag{24}$$

$$\left\langle\vec{m}\right\rangle = \left\langle\frac{\vec{f}_{tot}}{\Phi_0}\right\rangle - \left\langle\frac{\vec{f}_{ext}}{\Phi_0}\right\rangle = \frac{1}{2p}\frac{1}{N_{loops}}\sum_{loops}\left(\mathbf{M}\vec{j} - 2p\;\vec{f}_{ext} - 2p\;\vec{f}_{noise} + 2p\,\vec{n}\right) \tag{25}$$

We note that the external flux average, is simply equal to *f*, if, as is usually assumed, external field is uniform and flux noise have zero mean. We note that in static case Eq.(17) reduce to:

$$\frac{b_L}{2p}\sin\vec{j} = \mathbf{K}\vec{m} \tag{26}$$

this is the analogous of the Eq.(1) of Nielsen et. al. [58]. Explicit form can be obtained as follows:

$$\vec{m} = (\mathbf{L}\mathbf{M}^{\mathrm{T}})\left(\mathbf{M}\mathbf{M}^{\mathrm{T}}\right)^{-1}\mathbf{M}\frac{b_L}{2p}\sin\vec{j} \tag{27}$$

we note that there is an important difference respect to ref. [58]: if the mutual inductance effects are non-zero $\mathbf{L}\mathbf{M}^{\mathrm{T}}$ is not proportional to the identity matrix and this implies that magnetization in a given mesh depends on the currents in *all* the other branch of the array. To handle Eq.(27) one has to make explicit the dependence of the phases on the fluxes. This cannot be made in a simple way except for the case of the single loop because of phases that are arbitrary, not existing a one to one correspondence between phases and fluxes (so some additional hypothesis is necessary as symmetry hypothesis that permit to solve the equations as in the 1-loop case). Thus here we limit ourselves to solve the special case of the single loop and shown coincidence with Eq.(1) of [58]. Now for a single loop we suppose that by symmetry all phases are equal, this implies:

$$\mathbf{M}\vec{j} = \begin{pmatrix}-1 & 1 & -1 & 1\end{pmatrix}\begin{pmatrix} j \\ -j \\ j \\ -j \end{pmatrix} = -4j \tag{28}$$

where phase signs have been chosen to satisfy sum rule in Eq.(1). Substituting in the flux quantization equation we have:

$$\frac{f_{tot}}{\Phi_0} = \frac{1}{2p}\left(-4j + 2pn\right) \Rightarrow j = \frac{p}{2}n - \frac{p}{2}\frac{f_{tot}}{\Phi_0} \tag{29}$$

Moreover for a single mesh we have:

$$\mathbf{I}_{\mathrm{b}} = \mathbf{M}^{\mathrm{T}}\mathbf{I}_s = \begin{pmatrix}-1 \\ 1 \\ -1 \\ 1\end{pmatrix} I_s = \begin{pmatrix}-I_s & I_s & -I_s & I_s\end{pmatrix} \tag{30}$$

so using $\mathbf{MM}^{\mathbf{T}}=4$ and being in static conditions the (normalized) modulus of the screening current equal to $\sin j$ we find:

$$\left(\mathbf{MM}^{\mathbf{T}}\right)^{-1}\mathbf{M}\sin j = \frac{1}{4}\begin{pmatrix}-1 & 1 & -1 & 1\end{pmatrix}\begin{pmatrix}-\sin j\\ \sin j\\ -\sin j\\ \sin j\end{pmatrix} = \sin j \qquad (31)$$

finally being $\mathbf{L}=(1/4)\mathbf{M}$ and so $\mathbf{LM}^{\mathbf{T}}=1$, for a single loop, we obtain Eq.(1) of [58]:

$$m = (\mathbf{LM}^{\mathrm{T}})\left(\mathbf{MM}^{\mathrm{T}}\right)^{-1}\mathbf{M}\frac{b_L}{2p}\sin j = \frac{b_L}{2p}\sin j \Rightarrow m = \frac{f_{tot}}{\Phi_0} - \frac{f_{ext}}{\Phi_0} = \frac{b_L}{2p}\sin\left(\frac{p}{2}n - \frac{p}{2}\frac{f_{tot}}{\Phi_0}\right) \qquad (32)$$

From this last equation is evident that will be only four different magnetization states for a fixed values of total flux in the single loop (or for fixed external flux given by f_{tot}/Φ_0-m), being all others periodic repetition of the first four. The states, which are non-degenerate, will be classified as dia-magnetic or para-magnetic depending on the sign of the magnetization. Generally the preference for the system for one magnetization state depends on energetic considerations. In fact computing the Gibbs free energy $dG=-Idf_{ext}$ for the solutions of Eq.(32) will results that for $k<f<k+1/2$ with k integer the single mesh will be diamagnetic and for $k+1/2<f<k+1$ it will be paramagnetic. As we will show below this is true if values of b_L are relatively higher, i.e., if the array is strongly discrete or the HTC material we aim to model is substantially granular. This justifies also the use of full mutual inductance model to study this system. We note that this symmetric behavior in terms of frustation conducts to say that single mesh is in the 50% of cases diamagnetic and in the remaining 50% paramagnetic, i.e., there is not a prevalence of paramagnetism nor one of diamagnetism for what concerns the single mesh.

4.2 Simulated FC experiments over a 2D JJA

We solve Eq.(17) using the same method given in ref.[62]. In order to have paramagnetic response we need to study field cooled arrays, otherwise if we start from an arbitrary values of b_L different from zero and increase the external field via the parameter f in Eq.(17) than we end up with the classical Meissner state which is a well-known property of JJA equations as described in ref.[12]. Here we start directly with a non-zero frustation f in order to simulate field cooling (FC) and than increase b_L in steps until it reach the final value. In most of our runs this final value was 30 in order to compare model with experiments. To this end also dissipation controlled by b_C was set to 63 (cf. ref.[58]). Typical normalized times for each steps range from 80 to 400 normalized time units, for a total of about 30 steps until the maximum value of b_L is reached. The magnetization is sampled after the dynamical terms in Eq.(17) die out leaving the array in a static situation. This always happens except for integer values of frustation, i.e., for $f=k$ with k integer, where field cooled arrays appears to be unstable. We observe that also in our simulation the final magnetization is dependent of cooling rate as just observed in ref.[51]. This is

especially true for short cooling times, which generally gives stronger magnetization effects (and so larger field cooling susceptibility). In any case here we do not treat this problem which will be the subject of further investigations and use the largest possible cooling rates in order to make the numerical data only weakly dependent from cooling rate. Typical cooling rates in the experiments are obviously much larger than simulation times, also if their effective evaluation is difficult.

It will be assumed that thermal noise can induce a random distribution of phase-slips in the array when Josephson barriers are small, i.e., at the beginning of field cooling. This induces a random distribution of quantum number n in the array. To simulate this at the starting of simulation a random distribution of values of n is given. This procedure is different from that reported in ref.[51], as it uses explicit dependence of critical current by temperature, but it produce equivalent results as always the final state keep memory of first initial random distribution of flux quanta. We do not introduce explicit flux noise because barriers due to Josephson energy grows just in the first phase of the process and rapidly become larger than thermal fluctuations. The principal characteristic of noise free image, i.e., with n=0 for each mesh of the array, is its symmetry: meshes carrying high magnetization dispose symmetrically in the array. Anyway we note that also this very improbable distribution give roughly the same mean magnetization of the noised simulations. The variation of the mean magnetization for the change of distribution of quantum numbers was evaluated to be roughly of 2% at least for the number of statistical realizations we have simulated which here is of 4-5 for each frustation value. The result is the same for smaller array [71], where due to shorter CPU times the number of realization is roughly doubled.

In order to compare the array in-plane magnetization evaluated using Eq.(22) with the SSM read-out we need to calculate the far-field generated by the whole array and evaluate the flux in a loop of given area S and distance z above the array plane. The area of this last loop can be viewed as the "effective" area of the SQUID input loop and it is related at the resolution of the SSM. Details of this procedure have been described elsewhere [71]. Here we limit to observe that under general assumptions the JJA field can be calculated easily in the thin-wire approximation, which is just used in the calculation of mutual inductance, treating each branch as a finite length wire carrying a current given by Josephson term $\sin j$. Despite for real arrays this approximation can be rather crude it will work very well to reproduce all the qualitative aspect of the SSM images as we will show below.

With the increase of b_L the in-plane magnetization of the array meshes vary as shown in Fig.6 where we plot some of the first steps in b_L for f=1.2. Here we plot the number of mesh having a given magnetization, i.e., what we call in the following the magnetization histogram. We see that for lowest values of b_L the magnetization is weak as is expected being the screening currents zero in that limit. There are in general two peaks for $b_L > 1$ with magnetizations of different sign, i.e., paramagnetic and diamagnetic meshes coexist in the array. Paramagnetic meshes at $b_L = 1$ have a small (relative) value of paramagnetic magnetization and peaks are larger and not completely separated (some small intermediate values are found). For large values of b_L magnetization states tend to concentrate only around two values alone with different sign.

In Fig. 7a we show the two-dimensional magnetization at z equal to zero for a 20x20 array with f=1.2 evaluated by using Eq.(22). The array is prevailing diamagnetic, as light gray meshes are dominant except for few paramagnetic ones which will distribute rather

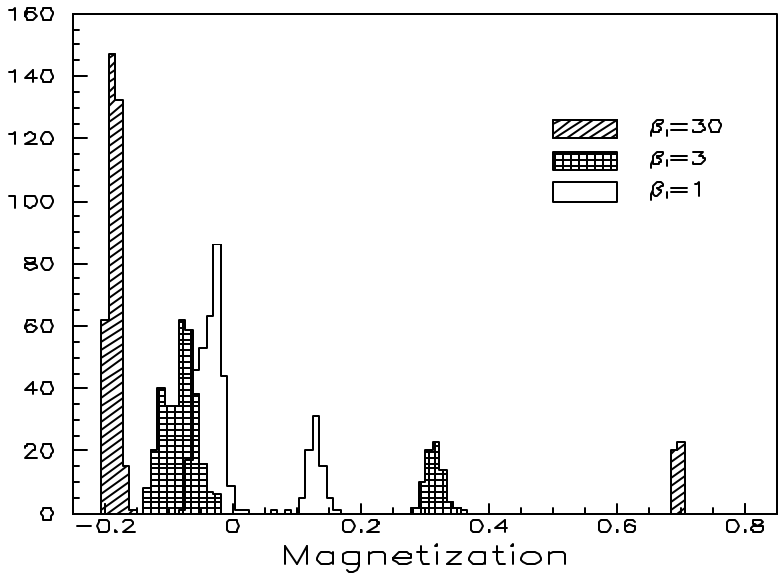

Fig.6. Magnetization histograms evaluated in plane at z=0 by Eq.(22) during the stepped field cooling process for a 20x20 arrays with f=1.2. Magnetization is normalized to flux quantum Φ_0. White pattern b_L=1; cross pattern b_L=3; hatch pattern b_L=30.

uniformly in the interior and on the boundary of the array. It is worth to note that values of the mean magnetization for each mesh of the array are nothing but the single mesh values that can be calculated by Eq.(32). This is clearly evident in Fig.8a where we report the final magnetization histogram at z equal to zero, i.e., the distribution of Fig.6 for the last value of b_L. As just noted above there are only two values of magnetization. It is important to note that the mean value of two partial histograms corresponds to single mesh states. The spread is the effect of mutual inductance coupling between array meshes. The mean magnetization $\langle m \rangle_0$ is −0.0907 which confirm that the array is diamagnetic. We note that the few paramagnetic meshes have larger magnetization than the diamagnetic ones, but they are too few to change the mean value.

In Fig.7b we report the magnetization evaluated as flux in the SQUID input loop at z equal one array mesh (this was roughly the distance used in ref.[58]). We set S equal to 1/100 of array mesh in order to map full details of magnetization above the array. Here the simulated image was obtained with a higher resolution with respect to that reported in [59]. It is evident that flux lines mix up over the array giving a more faint distribution of the paramagnetic sites. This image is much more similar to SSM read-out also if resolution is at the limit of best SSMs for typical mesh of 50x50 μm^2 reported in ref.[58]. In Fig.8b the corresponding histogram of magnetization evaluated at z equal one array mesh is given. As can be seen the two peaks merge in a single histogram, so the picture is very similar to that observed in experiments by Nielsen et al. [58]. The mean value $\langle m \rangle_1$ is −0.0171 at z=1, which is lower in magnitude with respect to z=0 case. This is justified by the fact that a careful examination of 3D far-field distribution shows that there are a good number of flux lines that close just around the array branch, these do not contribute to the total flux so mean magnetization goes rapidly down when the distance from the array increase.

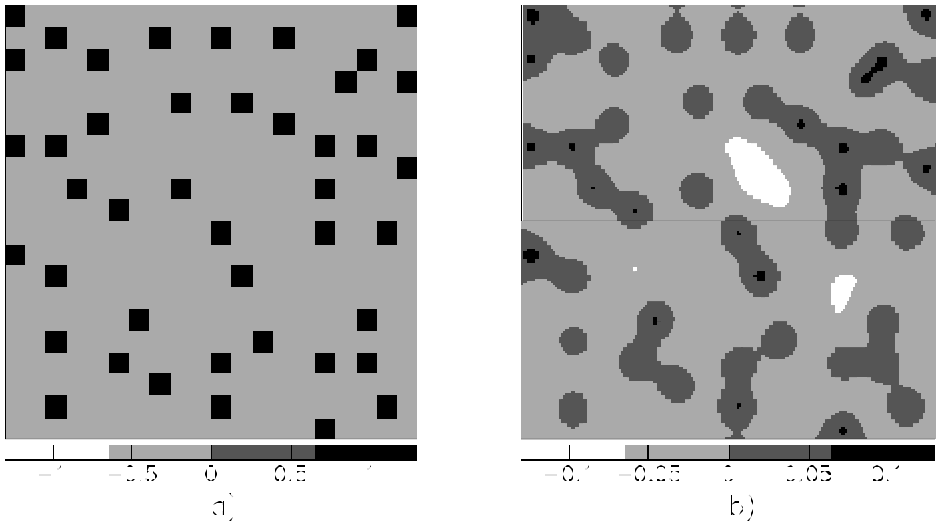

Fig.7 Two-dimensional magnetization for a 20x20 array at the end of field cooling process with b_L =30 and f=1.2. (a) the in-plane z=0 magnetization evaluated by Eq.(22); (b) the far-field magnetization at z=1 mesh with resolution equal to 1/100 of mesh. Light gray and white regions are diamagnetic, gray and dark gray paramagnetic.

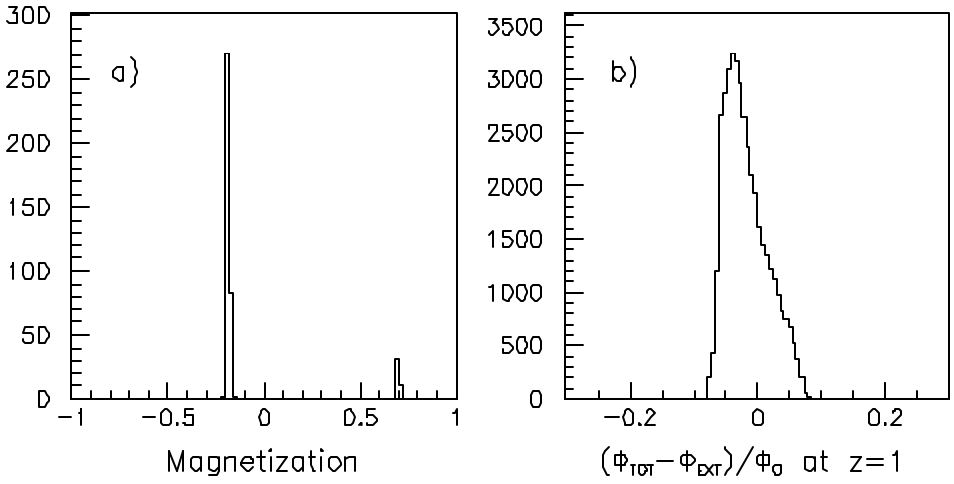

Fig.8 Magnetizat ion histograms for a 20x20 array at the end of field cooling process with b_L =30 and f=1.2. (a) the in-plane z=0 magnetization histogram evaluated by Eq.(22); (b) the far-field magnetization histogram at z=1 mesh with resolution equal to 1/100 of mesh.

Moreover some flux is also escaping from array edges. In Fig.9a is reported the z equal zero two-dimensional magnetization for the case f=4.8. As it is evident the situation is almost opposite of the previous one, the array is paramagnetic as gray meshes overcome the light gray ones. The z equal zero mean magnetization $\langle m \rangle_0$ is 0.163. This it is not surprising because the single mesh is paramagnetic just for the same frustation. Indeed the histogram reported in Fig.10a shows that the paramagnetic meshes have roughly the same

magnetization of single mesh and are larger in number with respect to diamagnetic ones. Exactly at the opposite of diamagnetic case the diamagnetic meshes have a stronger magnetization, but again they are too few to change the mean value. The paramagnetic response seems give more compact paramagnetic regions with respect to the diamagnetic case, so only few diamagnetic meshes appears near the boundary of the array. Thus paramagnetic array shows to be stronger than the corresponding diamagnetic. This view is confirmed by far-field analysis that is reported in Fig.9b for the two dimensional magnetization again at one mesh distance from the array plane and for the same resolution of 1/100 of mesh. The image is again reminiscent of experimental data. The

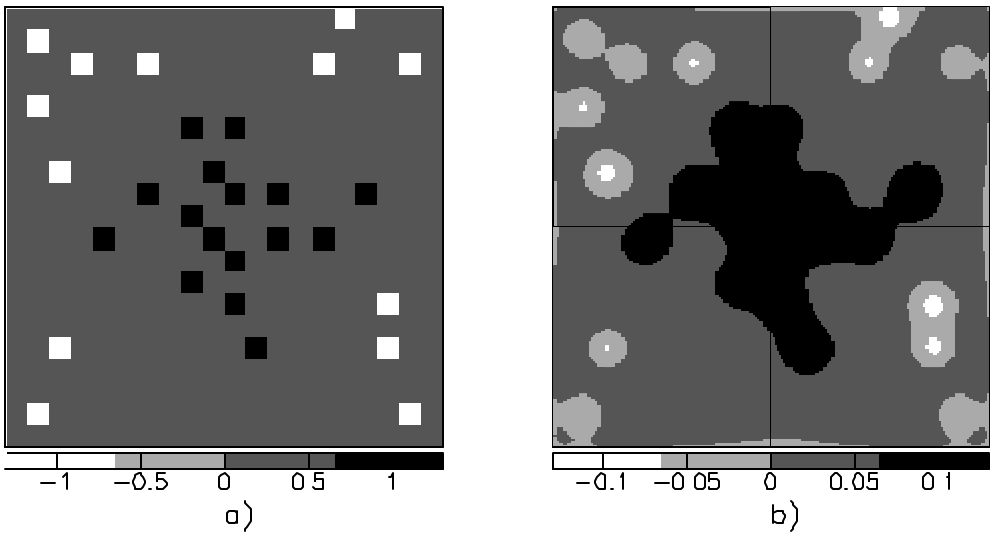

Fig.9 Two-dimensional magnetization for a 20x20 array at the end of field cooling process with b_L =30 and f=4.8. (a) the in-plane z=0 magnetization evaluated by Eq.(22); (b) the far-field magnetization at z=1 mesh with resolution equal to 1/100 of mesh. Light gray regions are diamagnetic, gray and dark gray paramagnetic.

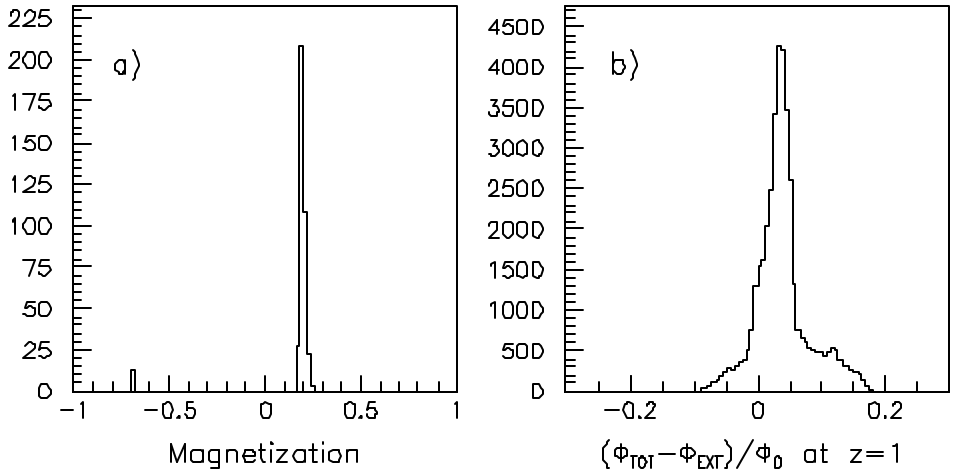

Fig.10 Magnetization histograms for a 20x20 array at the end of field cooling process with b_L=30 and f=4.8. (a) the in-plane z=0 magnetization histogram evaluated by Eq.(22); (b) the far-field magnetization histogram at z=1 mesh with resolution equal to 1/100 of mesh.

corresponding histogram is reported in Fig.10b where again the peaks merge and the mean magnetization $\langle m \rangle_1$ is 0.0393. We note that for $f=k+1/2$ with k integer, the single mesh states, dia- and paramagnetic, have the same (absolute) magnetization strength. So we expect for these frustation values to have roughly an equal number of diamagnetic and paramagnetic meshes. This really happens as is shown in Fig.11a for the in-plane magnetization in the case f=6.5, we see a roughly equal number of light gray and gray meshes. More significantly the histogram reported in Fig.12a, shows two similar peaks. Anyway the mean magnetization is $\langle m \rangle_0$=0.109, showing that the tendency is for

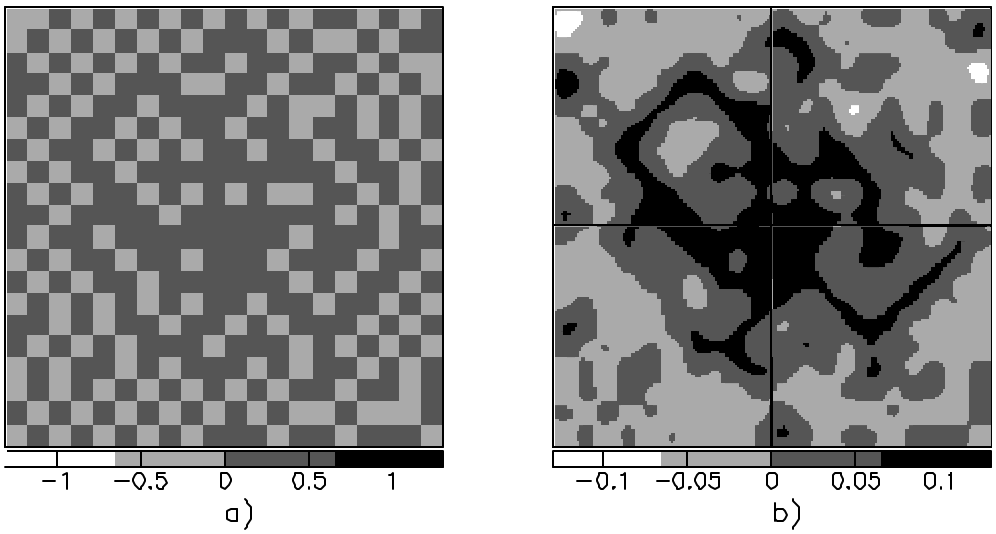

Fig.11 Two-dimensional magnetization for a 20x20 array at the end of field cooling process with b_L =30 and f=6.5. (a) the in-plane z=0 magnetization evaluated by Eq.(22); (b) the far-field magnetization at z=1 mesh with resolution equal to 1/100 of mesh. Light gray and white regions are diamagnetic, gray and dark gray paramagnetic.

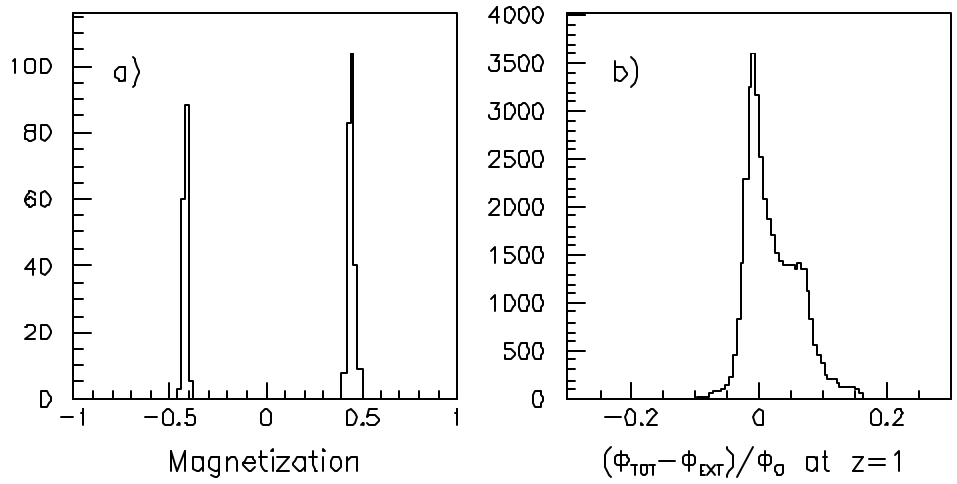

Fig.12 Magnetization histograms for a 20x20 array at the end of field cooling process with b_L=30 and f=6.5. (a) the in-plane z=0 magnetization histogram evaluated by Eq.(22); (b) the far-field magnetization histogram at z=1 mesh with resolution equal to 1/100 of mesh.

paramagnetism. The far-field image is shown in Fig.11b and far-field magnetization in Fig.12b. The far-field mean magnetization is lower $<m>_1$=0.0206.
The observed tendency of the arrays to reproduce the single mesh behavior is anyway not found at higher values of frustation. This is perhaps the most interesting question because it involves the justification of why paramagnetism is so easily developed in arrays. In fact experimental data show that for frustation slightly larger than 3 practically all the field cooled arrays response is paramagnetic rather than diamagnetic (cf. ref.s [58]-[59]). Thus the symmetry observed for the single mesh is broken and for most of the frustation values the field-cooled arrays show paramagnetism. Our simulations show the same results. In Fig.13a we show the in-plane two-dimensional magnetization for f=12.2. Again we observe a "sea" of diamagnetic meshes, as in the f=1.2 case, but with a higher number of paramagnetic meshes. This is observed in the z=0 histogram reported in Fig.14a. Being the magnetization strength of paramagnetic meshes larger we obtain a change in the sign of mean magnetization, i.e., the array is now paramagnetic with $<m>_0$=0.0754. The most clear sign of this is in the far-field magnetization: the merging of flux lines having the effect of reverse the aspect of the background sea of diamagnetic meshes expanding the stronger paramagnetic regions, so Fig.13b is more similar to Fig.9 than Fig.7. This is just what is observed in the experiments. We have simulated other cases for 10x40 and 10x10 array submitted elsewhere ([59]-[71]) plus a good number of tests for smaller N and different cooling times. All these simulations show always the behavior just described above. This collection of cases is resumed in Fig.15a where we report the z=1 mean magnetization. As it is evident arrays are paramagnetic for all value of f larger than about 3. The reason of the prevailing paramagnetism was described in Nielsen et al. [58]: paramagnetic states are preferred to diamagnetic ones because the array screens the field by generating diamagnetic currents on the array boundary and, as consequence, induces paramagnetic currents in the interior of the array, thus generating an overall paramagnetic

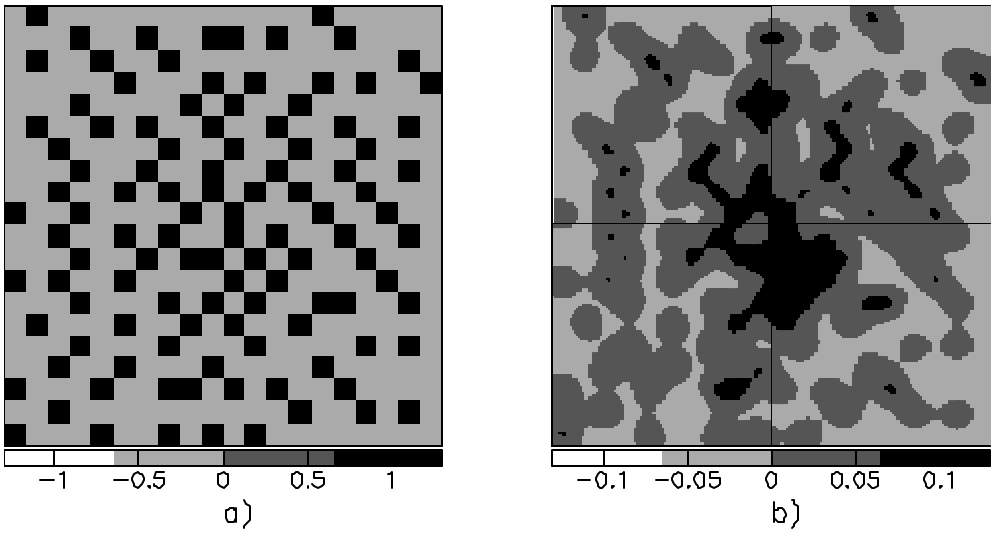

Fig.13 Two-dimensional magnetization for a 20x20 array at the end of field cooling process with b_L =30 and f=12.2. (a) the in-plane z=0 magnetization evaluated by Eq.(22); (b) the far-field magnetization at z=1 mesh with resolution equal to 1/100 of mesh. Light gray regions are diamagnetic, gray and dark gray paramagnetic.

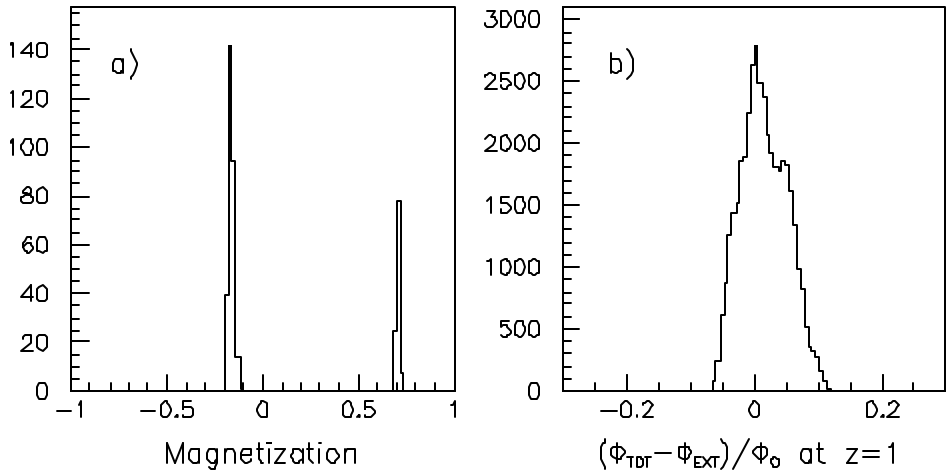

Fig.14 Magnetization histograms for a 20x20 array at the end of field cooling process with b_L =30 and f=12.2. (a) the in-plane z=0 magnetization histogram evaluated by Eq.(22); (b) the far-field magnetization histogram at z=1 mesh with resolution equal to 1/100 of mesh.

offset. In all Fig.s shown above, both dia- and paramagnetic, diamagnetic behavior prevails near the array edges. This agrees with the experiments on JJA where diamagnetism is found prevailing around the array boundary. To further support this view, we calculated the density of paramagnetic loops at the boundary ρ_b and bulk density of paramagnetic loops ρ_k of the array. The evaluated densities are reported in Fig.15b. Can be seen that for diamagnetic states densities are roughly equal for f=1.2 diamagnetic array, then for other values of f they become different clearly different.
Accordingly to above discussion the paramagnetic effect for large f is depending on the ratio between surface meshes and bulk meshes of the array, the first one grows like N, the second one like N^2, so for small arrays the effect goes to zero. Tests on smaller arrays show that paramagnetic behavior for $k<f<k+1/2$ is depending on the array dimension N. Smaller array shows a progressive decrease of mean magnetization which become negative at about N equal to 5, this is roughly the value predicted from Eq.(4) of Nielsen et al.[58] for b_L=30. We note also how analysis of surface and bulk densities for 10x40 and 20x20 arrays give roughly the same result, whereas for 10x10 the difference in densities is lower.

5.CONCLUSIONS

Though many successful descriptions of HTC superconductors have been made in terms of JJA today an exhaustive model of HTC superconductors cannot be thought exclusively in terms of JJA. Too many differences exists: HTC materials are multi-scale, i.e., they have several scales and types of granularity; are well described in terms of magnetization properties rather that current in circuits, are often noisy and disordered (though probably not at all the scales). So the interplay between HTC materials and LTC JJA arrays in the past years conducts us to the central question: how JJA circuital, local, single scale, noise-

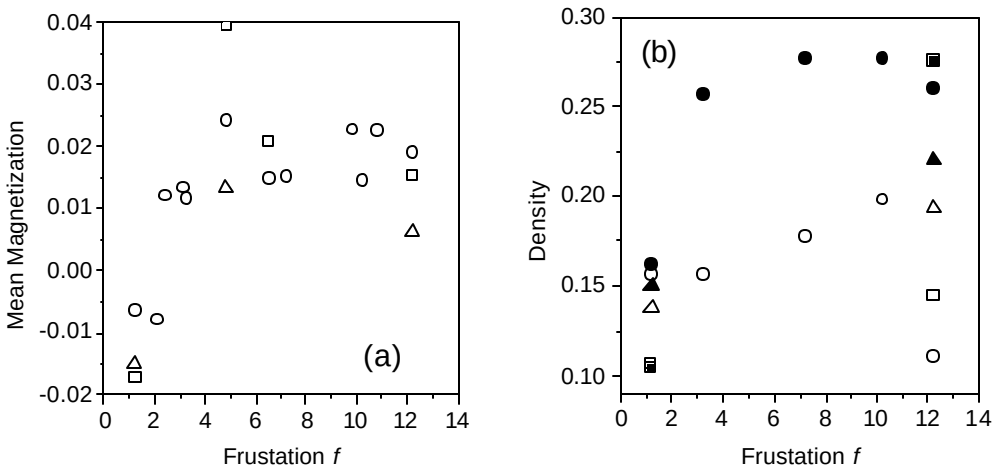

Fig.15 (a) Mean magnetization evaluated at z=1 results vs frustation for b_L =30. Squares are relative to above described figures; circles are relative to 10x40 arrays of ref.[59], triangles to 10x10 arrays of ref.[71]. (b) Bulk (black symbols) and surface (white symbols) densities of paramagnetic loops for the simulated arrays. Bulk density is the ratio between the number of paramagnetic meshes and the total mesh number. Boundary density is the ratio between the number of paramagnetic meshes on the array boundary and the number of meshes at the boundary. Circles are data from ref.[59], triangles from ref.[71] and finally squares are relative to above described data.

disorder free descriptions can be cut over non-local, multiscale, disordered and noisy HTC materials. A partial answer is the search for non-global descriptions, i.e., JJA cannot reproduce the whole dynamical phenomena shown by HTC materials, but can aid to do in determined circumstances. In this sense JJA are not a model of HTC, rather that we call an heuristic model, or, to say in a different way, HTC behavior can be described in terms of JJA in some well defined cases. On the other hand the progress toward "engineered" structures, the push for more clean, disorder free structures, e.g. capable of give higher critical currents or give arise to new quantum electronic devices (for example the development of q-bit based devices), are relevant facts that implies a future use of JJA models. In fact is just here that JJA models can be useful in view of their properties. In this paper we have treated 1D and 2D JJA in the above sense, i.e., using these models to clarify some of the questions relative to behavior of HTC materials. Much work and improvements will remain to be made. For 1D larger arrays with a random distribution of period n length can give a model able to better fit the existing data on YBCO films. Another important issue is the study of realistic boundary conditions for 1D JJA because as we have shown these influence directly their magnetization properties in the discrete case. For PME effect in 2D arrays, a number of open problems still remain to be analyzed. Among these we cite: simulations of larger arrays in order to make more detailed comparison with experiments and the study of the effect of cooling time and transient dynamics of the array. Recently the π-loops, i.e., array meshes with one (or more) π-junctions, have been also directly fabricated by HTC tricrystal samples showing interesting property [72]. So true π-loops HTC-arrays can in principle fabricated and tested.

Simulations of arrays with π-loops can aid to understand if their behavior is different or not from traditional (LTC)-JJA. In particular the symmetries shown by traditional JJA could be broken in π-loops arrays because the π-shift modify the single loop response by a half flux quantum as can be view from Eq.(32).

ACKNOWLEDGEMENTS

We thank warmly P.Barbara for having introduced us to the PME questions. We would like to thank also A.P.Nielsen and C.J.Lobb for their prompt comments and clever discussions about PME in LTC JJA. We are also in debt with G.Ghigo and E.Mezzetti for useful discussions and insights on the YBCO films magnetic properties. We acknowledge also P.Carelli, M.Cirillo, G.Filatrella and F.Tafuri for their comments and encouragement. Finally we would like to thank J.La Rosa for a critical reading of the manuscript. Finally we acknowledge support by Italian Ministry of University and Research MURST via Cofin2000 program *Dynamics and thermodynamics of vortex structures in supeconducting tunneling*.

Contact:
e-mail: rotoli@ing.univaq.it
web page: http://www.ing.univaq.it/energeti/research/Fisica/supgru.htm
or http://ing.univaq.it/energeti/research/Fisica/supgru.htm

REFERENCES

[1] K.A.Muller, M.Takashige and J.G.Bednorz, Phys.Rev.Lett. **58**, 1143, 1988; Y.Yeshurun and A.P.Malozemoff, Phys.Rev.Lett. **60**, 2202, 1988; M.Tinkham, Phys.Rev.Lett. **61**, 1658, 1988.
[2] P.Chaudhari, J.Mannhart, D.Dimos, C.C.Tsuei, J.Chi, M.M.Oprysko and M.Scheurmann, Phys.Rev.Lett. **60**, 1653, 1988.
[3] C.J.Lobb, D.W.Abraham, M.Tinkham, Phys.Rev.B **27**, 150, 1983.
[4] K.Nakajima and Y.Sawada, J.Appl.Phys. **52**, 5732, 1981.
[5] First papers demonstrating the coherent emission from JJA were A.K.Jain, K.K.Likharev, J.E.Lukens, and J.E.Sauvageau, Phys.Rep. **109**, 309, 1984 and S.P.Benz and C.J.Burroughs, Appl.Phys.Lett. **58**, 2162, 1992. Among most recent and interesting we signal P.Barbara, A.B.Cawthorne, S.V.Shitov and C.J..Lobb, Phys.Rev.Lett. **80**, 7575, 1999.
[6] C.S.Owen and D.J.Scalapino, Phys.Rev. **164**, 538, 1967.
[7] C.P.Bean, Phys.Rev.Lett. **8**, 250, 1962.
[8] F.Parodi and R.Vaccarone, PhysicaC **173**, 56, 1991.
[9] R.Fehrenbacher, V.B.Geshkenbein, G.Blatter, Phys.Rev.B **45**, 5450, 1992.
[10] A.Majhofer, T.Wolf and W.Dieterich, Phys.Rev.B **47**, 7481, 1993
[11] A.Petraglia, G.Filatrella and G.Rotoli, Phys.Rev.B **53**, 2732, 1996.
[12] D.Dominguez and J.V.José, Phys.Rev.B **53**, 11692, 1996.
[13] J.R.Phillips, H.S.J.van der Zant, J.White, T.P.Orlando, Phys.Rev.B **50**, 9387, 1994; ibid., 9380; J.R.Phillips, H.S.J.van der Zant, J.White, T.P.Orlando, Phys.Rev.B **47**, 5219, 1993.
[14] D.Reinel, W.Dieterich, T.Wolf and A.Majhofer, Phys.Rev.B **49**, 9118, 1994.
[15] C.Auletta, G.Raiconi, R.De Luca and S.Pace, Phys.Rev.B **51**, 12844, 1995.
[16] R. De Luca, S. Pace, C. Auletta and G. Raiconi, Phys.Rev.B **52**, 7474, 1995.
[17] R. De Luca, T. Di Matteo, A. Tuohimaa and J. Paasi, Phys.Rev.B **57**, 1173, 1998.
[18] J.V.José and G.Chu, Bull.Am.Phys.Soc. **39**, 378, 1994.
[19] C.J.Lobb, Physica **126**B, 319, 1984.
[20] T.S.Herbert, Y.Jun, R.S.Newrock, C.J.Lobb, K.Ravindarn, H.-K.Shiv, D.B.Hast, S.Elhamri, Phys.Rev.B **57**, 1154, 1998.
[21] S.Martin, A.T.Fiory, R.M.Fleming, G.P.Espinosa and A.S.Cooper , Phys.Rev. **39**, 9708, 1989;

[22] Yeh and C.C.Tsuei, Phys.Rev.Lett. **62**, 677, 1989; Ying and Kwok, Phys.Rev.B **42**, 2242, 1990.
[23] T.Chen and S.Teitel, Phys.Rev.Lett. **74**, 2792, 1995.
[24] H.S.Bokil and A.P.Young, Phys.Rev.Lett. **74**, 3021, 1995.
[25] M.P.A.Fisher and G.Grinstein, Phys.Rev.Lett. **60**, 208, 1988; M.P.A.Fisher, P.B.Weichman, G.Grinstein, D.S.Fisher, Phys.Rev.B **40**, 546, 1989.
[26] C.Bruder, R.Fazio and G.Schön, Phys.Rev.B **47**, 342, 1993.E.Roddick and D.Stroud, Phys.Rev.B **51**, 8672, 1995.
[27] A.van Oudenaarden and J. E.Mooij, Phys.Rev.Lett. **76**, 4947, 1996.
[28] S.Teitel and C.Jayaprakash, Phys.Rev.Lett **51**, 1999, 1983; C.Halsey, Phys.Rev.B **31**, 5728, 1985;
[29] P.L.Leath and W.Xia, Phys.Rev.B **44**, 9616, 1991.
[30] E.Granato and D.Dominguez, Phys.Rev.B **56**, 14671, 1997.
[31] M.Mombelli and H.Beck, Phys.Rev.B **58**, 12397, 1998.
[32] R.Kleiner, F.Steinmeyer, G.Kunkel and P.Müller, Phys.Rev.Lett. **68**, 2394, 1992.
[33] R.Kleiner and P.Müller, Phys.Rev.B **49**, 1327, 1994.
[34] A.Petraglia, N.F.Pedersen, P.L.Christiansen and A.V..Ustinov, Phys.Rev.B **55**, 8490, 1997.
[35] D. Winkler, N.Mros, A.Yurgens, and V.M.Krasnov, E.J.Tarte, D.T.Foord, W.E. Booij, and M.G.Blamire, Supercond..Sci.Technol. **12**, 1013, 1999.
[36] Cf. "Nano-Engineered Pinning Arrays" and "Vortex Dynamics in HTC Superconductors", in the special issue of Physica C, **332**, 1-4, May 2000.
[37] K.E.Gray, M.B.Field and D.J.Miller, Phys.Rev.B **58**, 9543, 1998.
[38] C.Reichhardt, C.J.Olson and F.Nori, Phys.Rev.B **58**, 6534, 1998.
[39] D.M.Feldmann, J.L.Reeves, A.A.Polyanskii, , A.Goyal, R.Feenstra, D.F.Lee, M.Paranthaman, D.M.Kroeger, D.K.Christen, S.E.Babcock, D.C.Larbalestier IEEE Trans.Appl.Supercond. **11**, 3772, 2001.
[40] D.Dimos, P.Chaudari, and J.Mannhart, Phys.Rev.B **41**, 4038, 1990; D.Dimos, P.Chaudari, J.Mannhart and F.K.Le Goues, Phys.Rev.Lett. **61**, 219, 1988.
[41] A.Gurevich and L.D.Cooley, Phys.Rev.B **50**, 13563, 1994;
[42] N.F.Heinig, R.D.Redwing, J.E.Nordman, D.C.Larbalestier, Phys.Rev.B **60**, 1409, 1999.
[43] I.Maggio-Aprile, C.Renner, A.Erb, E.Walker, Ø.Fischer, Nature **390**, 487, 1997
[44] J.E.Evetts, M.J.Hogg, B.A.Glowacki, N.A.Rutter, V.N.Tsaneva, Supercond.Sci.Technol. **12**, 1050, 1999.
[45] X.Y.Cai, A.Gurevich, I-Fei Tsu, D.L.Kaiser, S.E.Babcock, D.C.Larbalestier, Phys.Rev.B **57**, 10951, 1998.
[46] G.Ghigo, A.Chiodoni, R.Gerbaldo, L.Gozzelino, E.Mezzetti, B.Minetti, C.Camerlingo, G.Cuttone and A.Rovelli, Supercond.Sci.Technol. **12**, 1959, 1999.
[47] E.Mezzetti, A.Chiodoni, R.Gerbaldo, G.Ghigo, L.Gozzelino, B.Minetti, C.Camerlingo and C.Giannini, Eur.J.Phys.B **19**, 357, 2001
[48] G.Rotoli, C.De Leo, G.Ghigo, L.Gozzelino, C.Camerlingo, Int.J.Mod.Phys.B **14**, 3068, 2000.
[49] W.Braunisch, N.Knauf, S.Neuhausen, A.Grutz, A.Koch, B.Roden, D.Khomskii and D.Wohlleben, Phys.Rev.Lett. **68**, 1908, 1992; W.Braunisch, N.Knauf, G.Bauer, A.Koch, A.Becker, B.Freitag, A.Grutz, V.Kataev, S.Neuhausen, B.Roden, D.Khomskii and D.Wohlleben, Phys.Rev.B **48**, 4030, 1993.
[50] M.Sigrist and T.M.Rice, J.Phys.Soc.Jpn. **61**, 4283, 1992.
[51] D.Dominguez, E.A.Jagla and C.A.Balseiro, Phys.Rev.Lett. **72**, 2773, 1994.
[52] D.J.Thompson, M.S.M.Minhaj, L.E.Wenger, J.T.Chen, Phys.Rev.Lett. **75**, 529, 1995.
[53] P.Kostic, B.Veal, A.P.Paulikos, U.Welp, V.R.Todt, C.Gu, U.Geiser, J.M.Williams, K.D.Carlson and R.A.Klemm, Phys.Rev.B **53**, 791, 1996; A.K.Geim, S.V.Dubonos, J.G.S.Lok, M.Henini, J.C. Maan, Nature **396**, 144, 1998.
[54] A.E.Koshelev and A.I.Larkin, Phys.Rev.B **52**, 13559, 1995; V.V.Moschalkov, X.G.Qiu and V.Bruyndoncx, Phys.Rev.B **55**, 11973, 1999; P.S.Deo, V.A.Schweigert, F.M.Peeters and A.K.Geim, Phys.Rev.Lett. **79**, 4953, 1997.
[55] P.S.Deo, V.A.Schweigert, F.M.Peeters, Phys.Rev.B **59**, 6039, 1999.
[56] F.M.Araùjo-Moreira, P.Barbara, A.B.Cawthorne and C.J.Lobb, Phys.Rev.Lett. **78**, 4625, 1997; P.Barbara, F.M.Araùjo-Moreira, A.B.Cawthorne and C.J.Lobb, Phys.Rev.B **60**, 7489, 1999.
[57] W.A.C.Passos, F.M.Araùjo-Moreira, W.A.Ortiz, J.Appl.Phys. **87**, 5555, 2000.

[58] A.P.Nielsen, A.B.Cawthorne, P.Barbara, F.C.Wellstood, C.J.Lobb, R.S.Newrock, M.G.Forrester, Phys.Rev.B **62**, 14380-14383, 2000.
[59] C.De Leo, G.Rotoli, A.P.Nielsen, P.Barbara, C.J.Lobb, submitted to Phys.Rev.B, cond-mat/0103199
[60] M.Barahona, E.Trìas, T.P.Orlando, A.E.Duwel, H.S.J.van der Zant, S.Watanabe, S.H.Strogatz, Phys.Rev.B **55**, R11989, 1997.
[61] C.Lucheroni, Phys.Rev.B **55**, 6559, 1997.
[62] G.Filatrella, A.Petraglia and G.Rotoli, Eur.J.Phys.B **12**, 23, 1999.
[63] G.Grimaldi, G.Filatrella, S.Pace, U.Gambardella, Phys.Lett.A **223**, 463, 1996.
[64] S.Watanabe and S.H.Strogatz, PhysicaD **74**, 197, 1994; K.Wiesenfeld, Phys.Rev.B **45**, 431, 1992;
[65] M.Machida and H.Kaburaki, Phys.Rev.Lett. **71**, 3206, 1993.
[66] F.Lombardi, in web proceedings of Euroconference "Future Perspectives of Superconducting Josephson Devices", http://ing.univaq.it/energeti/research/Fisica/proc1.htm
[67] T.R.Lemberger, A.A.Pesetski and S.J.Turneaure, Phys.Rev.B **61**, 1483, 1999.
[68] D.Davidovic and L.Dobrosavljevic-Grujic, Phys.Rev.B **43**, 2809, 1991.
[69] P.H.E.Tiesinga, T.J.Hagenaars, J.E.van Himbergen, J.V.José, Phys.Rev.Lett. **78**, 519, 1997.
[70] C.De Leo and G.Rotoli, IEEE Trans.Appl.Supercond. **11**, 1219, 2001.
[71] C.De Leo and G.Rotoli, ISEC'01 Conference, Osaka 19-22 June 2001, see paper/poster preprint at http://ing.univaq.it/energeti/research/Fisica/supgru.htm
[72] R.R.Schulz, B.Chesca, B.Goetz, C.W.Schneider, A.Schmehl, H.Bielefeldt, H.Hilgenkamp, J.Mannhart, C.C.Tsuei, Appl.Phys.Lett. **76**, 912, 2000.